Methods Matter -- Standard Production Platforms For Recombinant AAV Can Produce Chemically And Functionally Distinct Vectors

Neil G. Rumachik[1,2], Stacy A. Malaker[1], Nicole Poweleit[3], Lucy H. Maynard[4], Christopher M. Adams[5,6], Ryan D. Leib[5], Giana Cirolia[4], Dennis Thomas[7], Susan Stamnes[8], Kathleen Holt[8,9], Patrick Sinn[8], Andrew P. May[4,11], and Nicole K. Paulk[4,10] *

[1] Stanford University, Department of Chemistry, Stanford, CA.
[2] *(currently)* Thermo Fisher Scientific, Ion Chromatography and Sample Preparation, Sunnyvale, CA
[3] University of California San Francisco, Department of Medicine, San Francisco, CA.
[4] Chan Zuckerberg Biohub, Genome Engineering, San Francisco, CA.
[5] Stanford University, Vincent Coates Foundation Mass Spectrometry Laboratory, Stanford, CA.
[6] (*currently)* Bruker Daltonics, Proteomics, San Jose, CA.
[7] Cold Spring Harbor Laboratory, Cryo-EM Core Facility, Cold Spring Harbor, NY.
[8] University of Iowa Carver College of Medicine, Viral Vector Core, Iowa City, IA.
[9] *(currently)* North Carolina Biotechnology Center, Raleigh-Durham, NC.
[10] University of California San Francisco, Department of Biochemistry & Biophysics, San Francisco, CA.
[11] (*currently)* Sana Biotechnology, South San Francisco, CA.

* Correspondence: Nicole Paulk, UCSF Department of Biochemistry & Biophysics, San Francisco, CA, Nicole.Paulk@ucsf.edu

Abstract

Different manufacturing approaches have been used in the production of recombinant adeno-associated virus (rAAV). We sought to characterize differences in rAAV vectors when produced by the two leading manufacturing platforms; live baculovirus infection of *Sf9* insect cells and transiently-transfected human HEK293 cells. We used multiple analytical approaches, including proteomic profiling by mass spectrometry, isoelectric focusing, cryo-EM, denaturation assays, next-generation sequencing of packaged genomes, human cytokine profiling in response to vector transduction, and comparative functional transduction assessments *in vivo* and *in vitro*. Our data support the following findings: 1) rAAV capsids have post-translational modifications (PTMs); 2) vector lot modifications included glycosylation, acetylation, phosphorylation, methylation and deamidation; 3) capsid PTMs differ when produced in either platform; 4) impurities were different in vectors when produced in either platform; 5) impurities can also have their own PTMs, including N-linked glycans; 6) capsid PTMs and impurities were seen across all rAAV serotypes, manufacturers, and purification types; 7) there was no difference in the packaged rAAV genome sequence in either platform; 8) baculovirus-*Sf9* vector lots have insect and baculoviral impurities and can have poorer packaging percentages than human-produced vector; 9) rAAV capsids have no significant structural differences when produced in either platform; 10) when given at the same vector genome dose, human-produced rAAVs can be more potent than baculovirus-*Sf9* vectors *in vitro* and *in vivo* (P<0.05-0.0001); and lastly, 11) regardless of the manufacturing platform, functional rAAV transduction is sexually dimorphic in the liver when administered IV, but not in skeletal muscle when administered IM. Our results demonstrate that baculovirus-*Sf9* and human manufacturing platforms can produce vector lots exhibiting chemical and functional differences. These findings were reproducible across numerous rAAV vendors, including commercial manufacturers, academic core facilities, and individual laboratories. These differences may have implications for receptor binding, trafficking, expression kinetics, stability, and immunogenicity.

Keywords: AAV, manufacturing, PTM, impurity, human, baculovirus, *Sf9*, insect, capsid, liver, sexual dimorphism, potency

Introduction

Adeno-associated virus (AAV) is a single-stranded DNA virus that is non-pathogenic to humans, exhibits low immunogenicity but high transduction efficiency, and is unable to replicate itself. Recombinant AAV can stably express gene products from either unintegrated episomes[1] in quiescent tissues, or via integration in actively dividing tissues[2] when designed with appropriate homology arms. Gene therapies and passive vaccines with rAAV are rapidly gaining attention and investment following the first rAAV therapy approval in the U.S. market. Nearly 200 rAAV clinical trials for various indications have been performed and numerous investigational new drug applications are in various stages of review at the Food and Drug Administration (FDA) and European Medicines Agency (EMA). The predominant rAAV production platform used for preclinical and clinical studies to date has been transient transfection of adherent human HEK293 cells[3]. However, growth limitations using adherent HEK293 cells have spurred manufacturing innovations to increase yields. A new platform utilizing live baculovirus infection of *Spodoptera frugiperda* (*Sf9*) insect cells produces an average of 7E4 vector genomes (vg)/cell[4-6]. Several recent clinical trials have used vector from this new platform. One difference between their preclinical validation and clinical trials was a transition in manufacturing platform from human HEK293 to baculovirus-*Sf9* when scale-up was needed. This often corresponded to an increased vector dose being administered to achieve relevant expression, and in some cases patients developed severe adverse events directly related to treatment[7,8]. Thus, while poised to revolutionize treatment of rare and common diseases

alike, a thorough characterization of differences in rAAV vector lots produced by the two manufacturing platforms was needed.

We characterized differences in vector lot composition at the genomic and proteomic levels. This was motivated by the fact that human and insect cells have different capacities to produce protein post-translational modifications (PTMs)[9]. Protein folding and PTMs can influence therapeutically administered proteins, including altering stability, targeting/trafficking, functional activity, and immunogenicity, all of which could affect rAAV functionality. Additionally, a concern in producing recombinant proteins for humans within insect cells is potential immunotoxicity. Humans can have acute allergenic reactions to non-mammalian N-glycans, as well as any N-glycan with an α1,3-fucose or β1,2-xylose linkage on the innermost N-acetyl glucosamine (GlcNAc)[10], both of which are modifications found on insect glycoproteins. Thus, certain insect glycoprotein impurities in baculovirus-S*f9* produced vector lots could pose potential risks.

Impurities of any kind are a known concern for all rAAV production methods. For example, the EMA assessment report for Glybera found the final vector lot impurities to be 'unacceptably high'[11]. Collectively, we therefore hypothesized that rAAV vector produced in the different manufacturing platforms may be compositionally diverse. Using an array of chemical, molecular, structural, bioinformatic, and functional assessment approaches, we characterized and report here the differences and similarities in rAAV vector produced by these two leading manufacturing platforms.

Results

The PTM landscape differs on rAAV vectors made using the human and baculovirus-Sf9 production platforms

We sought to determine whether rAAV capsids were post-translationally modified, and whether capsid PTMs or any host cell protein (HCP) process impurities differed between production methods and lots. We used deep proteomic profiling and liquid chromatography-tandem mass spectrometry (LC-MS/MS). To eliminate variables between human and baculovirus-*Sf9* platforms for comparative high-resolution MS/MS analysis, the following safeguards were implemented: a) all vector productions were carried out at the same time in one facility using identical equipment by the same individuals; b) vector lots were harvested, purified and underwent quality control together using the same assays; c) vector aliquots were frozen down identically and simultaneously; and d) aliquots were thawed together and prepared for analysis from lots that had been frozen for the same amount of time to eliminate effects of time spent frozen on potential PTM retention. One additional parameter that was important to control was the input DNA and backbone vector sequence itself. Recombinant AAV transfer vectors are encoded on plasmids for transfection in the human manufacturing platform and within a live baculovirus in the insect platform. To overcome this difference, we designed a custom transfer vector plasmid that has the necessary backbone components to be employed in both systems (**Figure S1**). Thus, the only differences remaining were that standard to each: human HEK293 cells were grown in adherent cultures and transiently transfected with three production plasmids, while insect *Sf9* cells were grown in suspension cultures infected with two second generation[5] recombinant baculoviruses needed to produce rAAV.

A set of rAAV8 productions was carried out and subdivided into four preparations for simultaneous purification: lots purified from cell lysates and media supernatant from each platform. LC-MS/MS analysis resulted in rAAV8 capsid protein coverage of 98.8% (human) and 97.3% (baculovirus-*Sf9*). Capsid modifications observed included O-linked glycans, N-terminal acetylation to start methionine, lysine/arginine acetylation, tyrosine/serine/threonine phosphorylation, lysine/arginine methylation, and aspartate deamidation (**Figure S2a-f**). PTMs were distributed along the entire polypeptide, and more PTMs were observed on baculo-rAAV8 capsids compared to those produced in human cells (**Figure 1a-e**). In addition, externally facing PTMs were more common than those in the capsid lumen in both platforms. However, the first 220 amino acids at the N-terminus of rAAV8 are disordered; thus, we lack structural data to classify the orientation of the PTMs there. Limited data suggests that these amino acids are located within the capsid[12,13]. Interestingly, several PTMs within this disordered and presumed lumenal region were shared between the human and baculo-rAAV8 lots: N-terminal acetylation on the initial start methionine, and phosphorylation on serines 149 and 153. These shared PTMs may play a conserved role in capsid-genome interactions or in intracellular trafficking following phospholipase A2 domain extrusion once in the endosome[14]. We confirmed the presence of all 16 recently reported deamidations which were observed on human cell-lysate purified rAAV8[15] on both human and baculo-rAAV8 cell lysate and media-purified preparations.

For the remaining residues 220-738 on rAAV8 for which robust structural data exists[16], those residues which are externally facing on the capsid may play roles in mediating blood clearance, antibody binding, cellular tropism, receptor binding, etc. We detected numerous PTMs within known external functional regions on rAAV8 (**Figure 1a-e**). For example, within the laminin receptor (LamR) binding region (residues 491-547 and 593-623)[17], we observed one shared and numerous differential PTMs between human and baculo-produced vectors. The one conserved modification was an O-GlcNAc on T494 within the LamR binding domain. However, baculo-rAAV8 had five different external modifications, compared to the two in human rAAV in this same domain. This included K530, which we detected to be capable of both acetylation and methylation on different capsids within the same vector lot. Interestingly, the C-terminal end of the human-produced vectors lacked observable PTMs, both internally and externally, while the baculo-produced rAAV8 vectors were often modified in this region, including an additional external O-GlyNAc on T663. No PTMs were detected in the known ADK8 neutralizing epitope region (586-591)[18]. Additionally, there are 8 lysines on the mapped structure of AAV8 VP3 predicted to be capable of ubiquitination[19]: K259, K333, K510, K530, K547, K569, K668 and K709. In human rAAV8 productions we observed no PTMs on or near any of these residues, while in baculovirus-*Sf9* productions we observed PTMs on two ubiquitinable lysines (K530 was methylated and acetylated; K709 was methylated), thus potentially blocking them from future ubiquitination.

Negative staining and transmission electron microscopy (TEM) confirmed that, despite identical purification procedures, human-produced rAAV had more full capsids, regardless of whether the rAAVs were purified from cell lysates or media supernatant (**Figure 1f-i**). We observed normal 1:1:10[20] ratios of VP1/2/3 by silver stain (**Figure 1j**) for each vector lot, however the baculovirus-*Sf9* vectors displayed additional truncated VPs as seen by others previously[21]. HCP impurities were present in all vectors, regardless of manufacturing platform, but were different between platforms (**Table S1**). Of concern, we observed *Sf9* insect HCP impurities with N-linked glycans (**Table 1**, **Figure S2g,h**). Cytokine profiling in primary human fibroblasts following transduction with each of the four vector lots by Luminex assay demonstrated that responses were more similar for human-produced rAAV8 vectors than for baculo-*Sf9* vector (**Figure S3**). Specifications on the viral lots are outlined in **Table S2**.

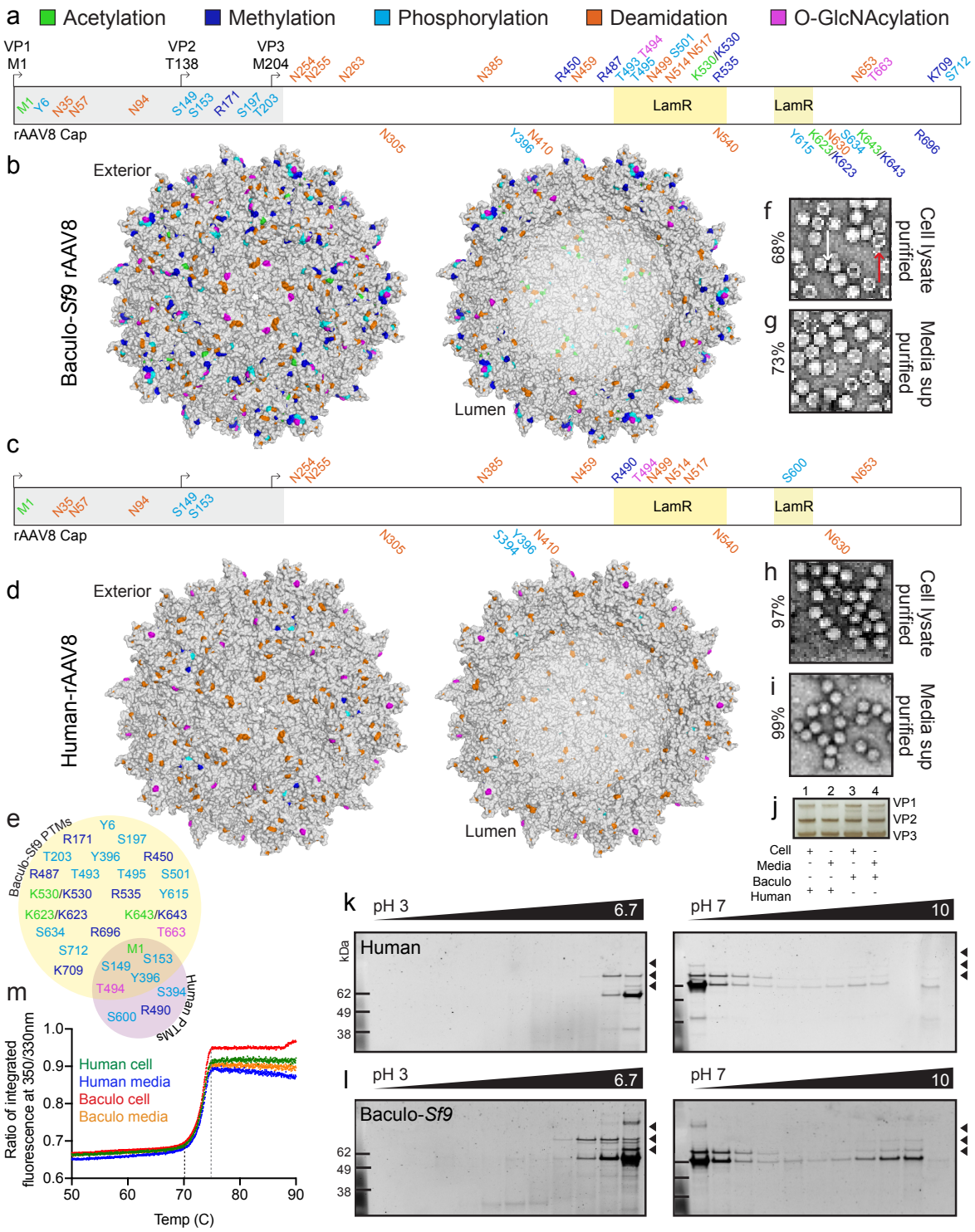

Figure 1: AAV vectors manufactured with the human and baculovirus-*Sf9* production platforms exhibit differential PTM profiles. (a) PTM identities and residue positions along the length of the rAAV8 polypeptide from N to C-terminus in baculo-*Sf9* vector. PTMs colored by type (acetylation = green, methylation = blue, phosphorylation = cyan, deamidation = orange, O-GlcNAcylation = magenta). Residues above the sequence are externally facing on the capsid. Residues below are lumenal or buried. Residues within the grey box from 1-220 represent the disordered region of AAV8 yet to be crystallized. The two regions for LamR binding (491-547 and 593-623) are highlighted in yellow boxes. **(b)** Cumulative capsid PTMs observed from all baculo-*Sf9* rAAV8 lots, purified from both cell lysates and media. Same color code as in (a). **(c)** Same as (a) but with human-produced rAAV8. **(d)** Same as (b) but with human rAAV8. **(e)** Shared and unique capsid PTMs for rAAV8 produced in the baculo-*Sf9* (yellow) and human systems (purple). Same color code as in (a). Excluded are deamidation degradation marks which were universally shared. **(f)** Negative staining and TEM imaging of baculo-*Sf9* rAAV8 cell-purified vector. White arrow denotes a full capsid, red arrow denotes an empty capsid, for reference for panels f-i (percent full capsids noted to the left). **(g)** Same as (f) but media purified vector. **(h)** Same as (f) but with human rAAV8 cell purified vector. **(i)** Same as (h) but with media purified vector. **(j)** Silver stain of capsid VP species present in vector lots from panels f-i. **(k)** 2D gel images from human-produced rAAV8 from pH 3-10. VP1 (87 kDa), VP2 (72 kDa), and VP3 (62 kDa) bands denoted with black arrowheads. **(l)** 2D gel images from baculo-*Sf9* produced rAAV8. **(m)** Thermal capsid melt curves for rAAV8 vectors shown from 50-90^{0}C, full melt curves from 30-95^{0}C are in Fig S8a. Tm initiation = dashed black line; final Tm = dashed grey line.

To ensure reproducibility, an independent set of experiments was performed with four new lots of rAAV8 prepared according to the same protocols, and results were consistent with initial experiments (**Figure S4, Table S3**). To determine whether the baculo-*Sf9* rAAV results would be different with first generation[4] baculoviral constructs—as were used in the rAAV1-LPL trial for Glybera[22]—we prepared another four lots of rAAV8, only now using the original baculoviral support constructs for the baculovirus-*Sf9* productions. Here again, results with first generation constructs were consistent with those reported for the two former replicates using second generation constructs (**Figure S5, Table S4**). Host cell ferritin contamination of suspension-grown rAAV preparations is known[23], and was seen in the baculovirus-*Sf9* lots.

2D gel electrophoresis independently confirmed vector differences

To validate differences observed at the proteome level from LC-MS/MS, we performed 2D gel electrophoresis (in-solution isoelectric focusing followed by SDS-PAGE) on four paired rAAV8 vector samples from Figure 1. Briefly, samples were loaded into wells above a pre-cast pH gradient gel strip and run in the presence of current such that proteins migrated through the gel to the well where the isoelectric point (pI) matched the well pH. After migrating, samples in each well were removed and run in separate lanes on a standard SDS-PAGE gel to separate by size in the second dimension (**Figure S6**). Chemical differences affecting pI in capsid proteins manifest as lateral banding, and we observed VP1/2/3 proteins that migrated beyond the well corresponding to the natural pI of rAAV8 (pI 6.3)[24]. These bands reflect differences in PTMs or potentially other unidentified modifications (**Figure 1k,l**). At different physiological conditions (pH/temperature), rAAV can undergo conformational changes due to phospholipase A_2 catalytic domain flipping within VP1[24]. However, this would not result in the observed lateral banding, as conformational changes do not significantly alter the net charge, and thus pI, of a protein[25]. Additionally, lateral banding was observed predominantly on VP3, which lacks the phospholipase domain. Of note, VP3 bands had substantially greater lateral banding than VP1 or VP2, possibly due to its higher abundance. To rule out the potential influence of host cell proteases being responsible for the banding patterns seen by 2D gel electrophoresis, an independent control was run wherein rAAV8 samples were treated with and without protease inhibitors and run as before to ensure the banding patterns remained unchanged. No difference was seen between treatments (**Figure S7a**) confirming the previous findings that banding patterns were not due to contaminating proteases. To determine if lateral banding resulted from rAAV cleavage products or substantial loss of PTMs, immunoblot analysis of the 2D gels was performed with an anti-AAV VP1/2/3 antibody[26]. Immunoblots confirmed that lateral banding was rAAV capsid proteins and that vertical banding was likely attributable to HCPs (**Figure S7b,c**). To determine whether differences imparted by the capsid PTMs could influence capsid stability, thermal melt curves were performed and no differences were found between baculovirus-*Sf9* and human-produced rAAV8 vectors (**Figures 1m, S8a**). All displayed standard rAAV8 melt curves initiating at 70^0C and completing at 75^0C, similar to rAAV8 vector lots from other academic and commercial providers (**Figure S8b-d**) for each platform. Of note, every serotype, regardless of method of production, has a unique capsid Tm that can vary from as low as ~72^0C for rAAV2 to as high as ~91^0C for rAAV5, with other common serotypes falling in between (**Figure S8b-d, Table S5**).

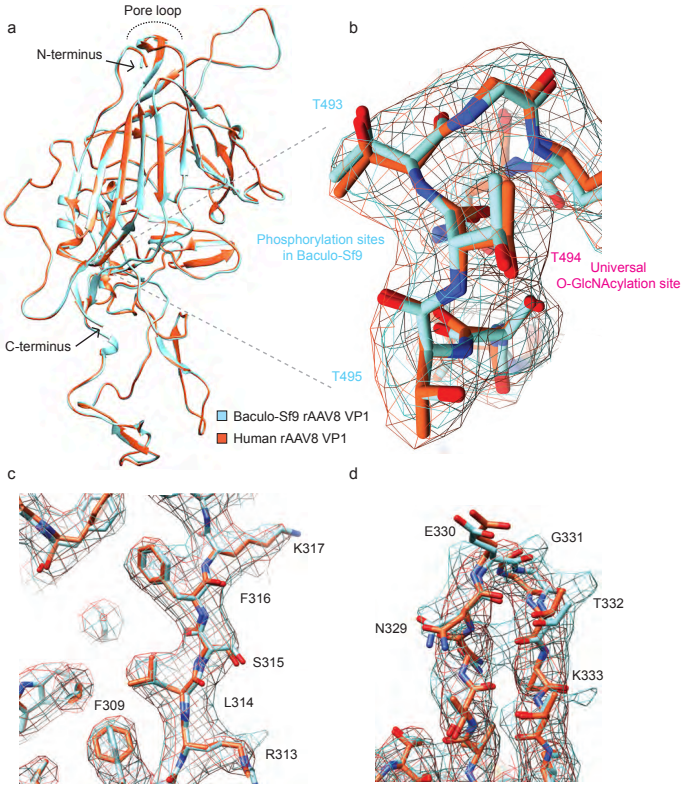

Figure 2: Human and baculovirus-*Sf9* production platforms produce rAAV capsids with similar structures. (a) Overlay of an individual VP1 chain from a human (red-orange) and baculo-*Sf9* (cyan) full rAAV8 capsid highlighting an absence of macro-level differences. Key structural landmarks are shown. **(b)** Magnified overlay of the LamR binding region from a human (red-orange electron density caging) and baculo-*Sf9* (cyan) full rAAV8 capsid highlighting residues capable of post-translational modification as determined by LC-MS/MS. **(c)** Magnified overlay depicting potential side-chain level structural differences in phenyl ring orientations between human (red-orange) and baculo-*Sf9* (cyan) rAAV8. **(d)** Magnified overlay of a human (red-orange) and baculo-*Sf9* (cyan) rAAV8 capsid single cylinder loop depicting minor potential side-chain level differences.

Presence of capsid alterations and HCP impurity levels are consistent within platforms across serotypes

To understand whether the former results with rAAV8 were serotype-specific or inherent to each platform, an identical set of rAAV1 preparations was produced and subdivided into four separate groups for simultaneous purification as was done for rAAV8. LC-MS/MS results, with an average of 87.9% (human) and 83.4% (baculovirus-*Sf9*) capsid coverage, showed that rAAV1 vector capsids are also post-translationally modified, and that the types and frequencies of each again differed between the two platforms (**Figure S9a-e**). Four rAAV1 PTMs within the disordered N-terminal region of the capsid were shared between the human and baculo-rAAV1 vectors: N-terminal acetylation on the initial start methionine, methylation of lysine 61, and phosphorylation on serines 149 and 153. For the remaining residues 217-736 on rAAV1, we detected numerous PTMs within known capsid antigenic motifs that react with known neutralizing antibodies against rAAV1 (456-AQNK-459), (492-TKTDNNNS-499), and (588-STDPATGDVH-597)[27]. One PTM was detected within the 4E4 neutralizing epitope residue (456-459 and 492-498)[28,29], and several additional PTMs were detected near the 5H7

Source	*Sf9* HCP impurity peptides with N-linked glycans	Unmodified peptide mass (Da)	Modified peptide mass (Da)	Hex NAc	Hex	Me-HexA	Fuc
Cell lysate	**N**YTVELHELEALAK	1629.8483	2668.2303	2	3		1
			2871.3117	3	3		1
			2506.1707	2	2		1
			2696.2244	2	2	1	1
			2522.1711	2	3		1
			1978.9856	1			1
			1832.9276	1			
	NYTVELHELEALAAK	1700.8854	1903.9647	1			
	A**N**YTVELHELEALAK	1700.8854	1903.9647	1			
	N(+28)YTVELHELEALAK	1657.8796	1860.9589	1			
			2696.2200	2	3		1
Media	**N**YTVELHELEALAK	1629.8483	2668.2303	2	3		1
			2871.3117	3	3		1
			2506.1757	2	2		1
			1978.9881	1			1
			2522.1714	2	3		
			2696.2214	2	2	1	1
			1832.9298	1			
	K**N**YTVELHELEALAK	1757.9436	2650.2657	2	3		
			2796.3262	2	3		1
			2999.3988	3	3		1
	AK**N**YTVELHELEALAK	1828.9803	2721.3024	2	3		
			2867.3606	2	3		1
	NYTVELHELEALANR	1771.8973	2810.304	2	3		1
	NYTVELHELEALNR	1700.8602	2739.2646	2	3		1
			2593.2048	2	3		
	NYTVELHELEALAAK	1700.8854	1903.9647	1			
	A**N**YTVELHELEALAK	1700.8854	1903.9647	1			

Table 1. HCP impurities with N-linked glycans from baculovirus-*Sf9* produced preparations of rAAV8. N-linked glycans (modified residue = **bold**) identified on the common *Sf9* HCP impurity ferritin identified by LC-MS/MS for rAAV8 from both cell lysate and media-purified vectors. Excluded from the list are common process contaminants that occur in routine sample preparation (human keratin, trypsin, etc.), impurities with mutations/aberrations such that they didn't map to known proteins by BLASTp search, and any modification which could not be site-localized. The unmodified and modified peptide masses are shown, as well as the number of glycan moieties each modified mass represents. HexNAc = N-acetylhexoseamine; Hex = hexose; Me-HexA = methylated hexuronic acid; Fuc = fucose; Da = dalton. No HCP impurity peptides in the human rAAV8 preparations were observed with N-linked glycans.

neutralizing epitopes (494, 496-499, 582, 583, 588-591, 593-595, 597), as well as the ADK1a neutralizing epitope (500). Additionally, there are 11 lysines on the mapped structure of rAAV1 VP3 predicted to be capable of ubiquitination: K258, K459, K491, K493, K508, K528, K533, K545, K567, K666 and K707. In both human and baculovirus-*Sf9* rAAV1 productions we observed PTMs on two ubiquitinable lysines where K459 and K528 were methylated.

Here again, HCP impurities were present and different between platforms (**Table S6**), and *Sf9* insect HCP impurities were detected with N-linked glycans (**Table S7**). Specifications on the viral lots are outlined in **Table S8**. Negative staining and TEM imaging confirmed that, despite identical purification procedures, human-produced rAAV1 had fewer HCP impurities and reproducibly full capsids compared to baculovirus-*Sf9* vector preparations (**Figure S9f-i**). We observed normal VP1/2/3 ratios by silver stain (**Figure S9j**), and again did not detect significant differences in thermal capsid stability (**Figures S9k, S8e**).

rAAV capsids are structurally similar when produced by different manufacturing platforms

Having demonstrated differences in vector lot composition at both the capsid PTM and vector lot impurity levels when produced by different production platforms, we next wanted to assess whether the global capsid structures differed by transmission electron cryomicroscopy (cryo-EM). To fairly assess any potential structural differences, we first needed comparable capsid structures from identically purified vector lots subjected to cryo-EM using the same methodology. Thus, we generated four new cryo-EM structures of full and empty rAAV8 capsids from each manufacturing platform (**Table S9**). Despite differential PTM deposition, no significant differences were observed between the averaged capsid structures at the resolutions achieved (3.3-3.6Å) (**Figures 2, S10**).

Common serotypes of rAAV experience capsid PTM deposition and have HCP impurities

Having shown that standard rAAV production methods produce capsids decorated with PTMs, we wanted to determine whether this was specific to the two serotypes tested or a generalizable phenomenon. To assess the presence and/or absence of capsid PTMs across serotypes, we sourced a panel of common rAAV serotypes 1-8, produced in either the human or baculovirus-*Sf9* systems (**Table S10**) from a single manufacturer to minimize potential production variation, and performed LC-MS/MS. We observed that all rAAV capsids, regardless of serotype or manufacturing platform, possessed capsid PTMs (**Table S11**). Additionally, all vector lots had HCP impurities (**Table S12**), and some were detected with N-glycosylations (**Table S13**).

Capsid PTM deposition and HCP impurities are universally seen across production scale, purification method, facility and production platform

Up to this point, vector lots from a single manufacturing facility in highly controlled production and purification settings were assessed. We next wanted to determine whether these findings were generalizable across

different production batches and manufacturing sites. To examine this, we sourced rAAV vector lots from an array of production facilities spanning private industry, leading academic core facilities, government consortia and individual academic laboratories (**Table S14**). Here the intent was not to rigorously control the production and purification parameters, but rather to determine the extent of modifications and impurities with samples obtained from vendors supplying vector to scientists working at every stage in the R&D pipeline. LC-MS/MS demonstrated that capsid PTMs and HCP impurities were universal (**Tables S15-16**), regardless of the scale of production, purification method used, manufacturing facility, or production platform. Cumulative comparative HCP impurity analyses on all vector lots tested to date using gene ontology analysis highlighted trends in HCP impurity types (**Figure S11** and **Tables S17-19**). Interestingly, the most common human impurities were related to nucleic acid and protein binding for RNA processing, the most common *Sf9* impurities were related to endopeptidase activity and proteolysis, while baculoviral impurities were either structural in nature or pertaining to viral escape.

Lastly, despite the presence of putative endoplasmic reticulum (ER) signal peptides[30] at the N-terminus of VP1 on all common rAAV serotypes (**Table S20**), our LC-MS/MS data show that rAAVs are often N-terminally acetylated, a PTM known to block ER translocation of polypeptides in eukaryotes[31]. The potential ER-exclusion is consistent with the glycosylation patterns seen on rAAV capsids which have been observed to have simple O-GlcNAc modifications (deposited in the nucleus or cytoplasm), but lack N-glycans or complex O-glycans (deposited in the ER/Golgi).

Vectors produced with the human manufacturing platform exhibit greater potency in vitro

Having established PTMs and HCP impurities as key differences in rAAV vector lots, we next sought to determine whether vector potency differed between manufacturing methods. We setup comparative expression experiments in a panel of cell lines spanning different species, cell types, differentiation states, and immortalization status. Immortalized human HEK293T and Huh7 cells, primary human fetal fibroblasts, primary human iPSCs, and immortalized mouse C2C12 myoblasts were transduced with Firefly Luciferase (FLuc) vector lots (human-cell, human-media, baculo-cell, and baculo-media AAV1-EF1α-FLuc) to measure potential expression differences. FLuc assays confirmed significant potency differences in all cases, regardless of species or cell type, with human-produced vectors outperforming insect-produced vectors in all cases ($P < 0.05$-<0.0001) (**Figure 3a**). To validate that expression differences were not due to differential packaging efficiency, we developed a next-generation sequencing (NGS) protocol called Fast-Seq[32] to sequence packaged rAAV genomes, including ITRs. Fast-Seq validated that all vectors used in the potency assessments had no difference in the packaged genomes between any vector lot by either production method (**Figures 3b, S10,** and **Tables S21-22**). These findings substantiate that the observed expression differences were not due to differences in the packaged genomes between vector lots.

To assess whether host cell protein impurities and/or empty capsids were poisoning the potency of the baculovirus-*Sf9* preparations, we setup an *in vitro* spike-in experiment with rAAV1-FLuc. A fixed amount of standard genome-containing vector was spiked with purified lots containing only empty capsids and their associated HCPs at different ratios (100:0, 90:10, 50:50, 10:90, 0:100) to determine whether the signal drop-off would correlate with the percent of spike-in material. Human-produced rAAV1-FLuc responded linearly when empty human-produced rAAV1 was spiked in (**Figure 3c**). In contrast, baculo-produced rAAV1-FLuc signals dropped off precipitously once >10% of the total vector came from empty vector (**Figure 3d**). This supports the hypothesis that the presence of insect/baculoviral impurities and/or empty capsids in baculovirus-*Sf9* preparations is influencing the potency of these vector preparations.

Vectors produced by different manufacturing platforms differentially transduce skeletal muscle in vivo

To assess potential potency differences *in vivo*, we setup a transduction comparison with the following parameters: a) age-matched mice to prevent confounding effects of age-related transduction; b) mice of each sex were treated; c) the same ssAAV-CMV-FLuc-SV40pA transfer vector was used to facilitate comparisons between production methods and manufacturers; d) vectors were sourced from two popular manufacturers for each platform (viral lot specifications in **Table S23**); e) all mice were injected intramuscularly (IM) by the same person on the same day and housed in their own cage per treatment to prevent cross-contamination by vector shedding; f) we used the same serotype (rAAV1) and method of injection (IM) as was used clinically for Glybera[11]; g) a low dose of 5e10 vg/mouse was chosen as this is sufficient to provide adequate FLuc signal but not so high that the maximal expression would already be reached thereby masking any potential potency differences. Twelve mice (6 male and 6 female) were injected IM and live-imaged weekly for FLuc expression (**Figures 3e, S13a**). Time course results revealed that human-produced rAAV1 achieved significantly higher skeletal muscle expression than baculovirus-*Sf9* produced rAAV1 in both sexes (P values <0.0001 at week 8) (**Figures 3g, S13b**).

To determine whether these potency differences were restricted to IM delivery of rAAV1, we repeated the same experiment with rAAV8—a serotype currently being tested as an intramuscular HIV passive vaccine vector[33], despite reports of poor transduction in human skeletal muscle[34] and other human tissues[35,36], as well as high neutralizing antibody levels in HIV+ individuals[37]. Here again, twelve mice (6 male and 6 female) were injected IM with 5e10 vg of ssAAV8-CMV-FLuc vector and live-imaged weekly for FLuc expression (**Figures 3f, S13c**). Human-produced rAAV8 achieved significantly higher expression than baculo-rAAV8 in both sexes (P values <0.0001 at week 8) (**Figures 3h, S13d**).

rAAV vectors exhibit significant sexually dimorphic functional transduction differences in liver expression in vivo

Administration of rAAV IM is typically only done when treating muscle disorders or when using muscle as a secretion depot for passive vaccines[34]. Many gene therapy trials administer vector intravenously (IV) to facilitate distribution to internal organs not easily accessible by direct injection. Thus, we next assessed whether the potency differences seen with IM administration would be recapitulated with IV administration of human and baculovirus-*Sf9* produced rAAV. For this deeper set of comparisons, we utilized vector lots produced from a single facility and our custom dual-use transfer vector (**Figure S1**) to even more stringently control for variations between the two production platforms. Twenty-four mice (12 male and 12 female) were injected IV with 5e10 vg/mouse of ssAAV1-EF1a-FLuc produced in either the human or baculo-*Sf9* system and live-imaged weekly for FLuc expression (**Figure 4a**). Results highlighted several key findings. First, human-produced rAAV1 achieved higher expression than baculo-*Sf9* produced rAAV1 over the duration of the time course ($P < 0.05$-0.0001) (**Figure 4c**). Second, significant sexually dimorphic differences were seen with both vector types and purification sources, where males experienced greater functional liver transduction than females ($P < 0.05$-0.0001).

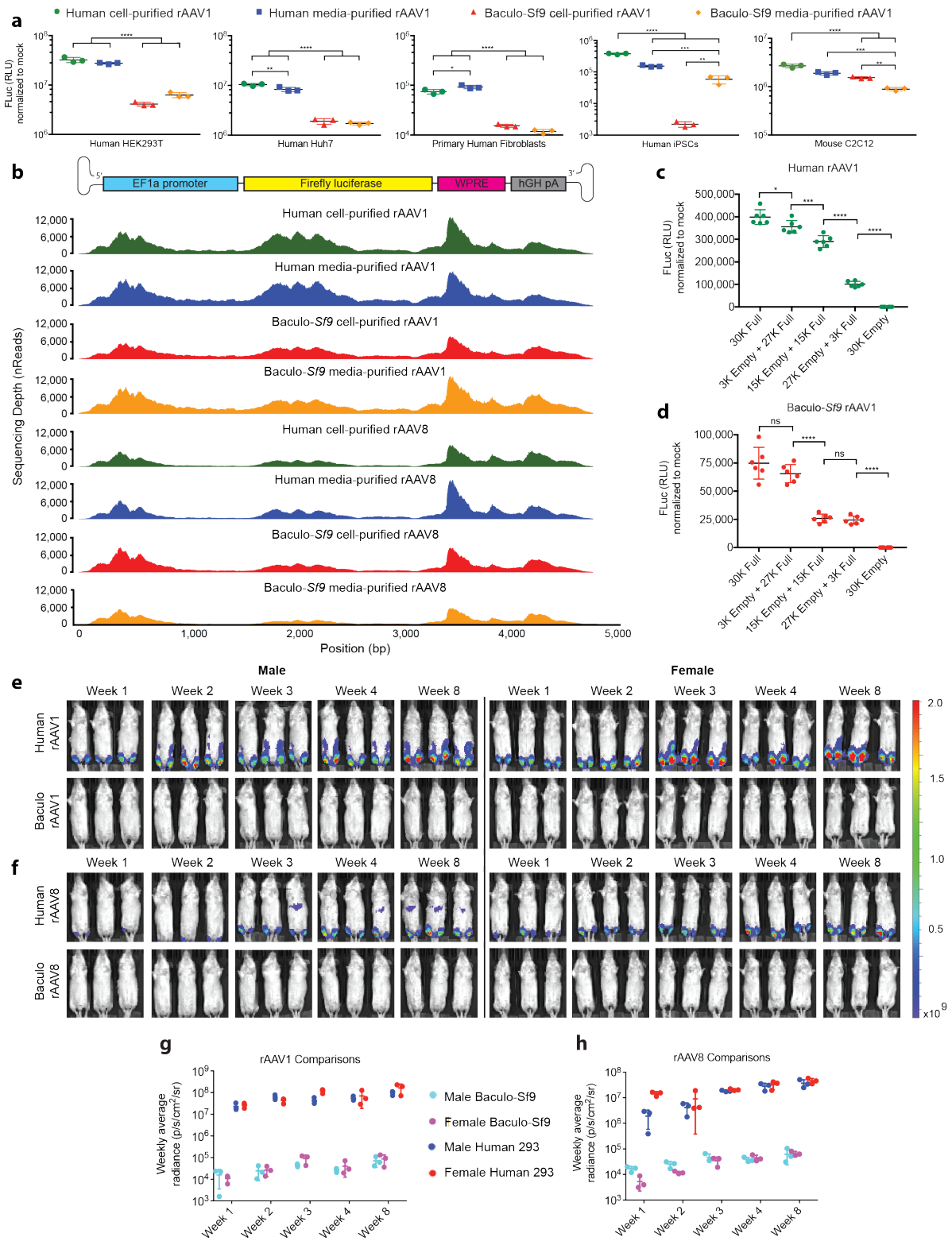

Figure 3: rAAV vector produced with the human HEK293 platform is more potent *in vitro* and *in vivo*. (a) Immortalized human HEK293T and Huh7 cells, primary human fibroblasts, primary human iPSCs, and immortalized mouse C2C12 myoblasts were transduced with ssAAV1-EF1α-FLuc at MOI 80K. FLuc assays were performed on cell lysates 3 days post-transduction and normalized to mock transduced wells. **(b)** NGS sequence plots of depth and coverage of packaged rAAV genomes, including ITRs, validating that genomes from human and baculo-*Sf9* produced vectors are identical and full-length. **(c)** HEK293T cells were transduced with varying ratios of full:empty human-produced ssAAV1-EF1α-FLuc with the total capsid content kept constant at MOI 30K, while the ratio of full:empty varied. FLuc assays were performed on cell lysates 3 days post-transduction and normalized to mock-transduced wells. Each green dot represents one replicate; mean +/- SD shown. **(d)** Same as (c) expect using baculo-*Sf9* AAV1. **(e)** Time course functional transduction FLuc data from human and baculo-*Sf9* ssAAV1-EF1α-FLuc after IM administration (5E10 vg/mouse) in age-matched male and female sibling Balb/SCID mice. Mean radiance (p/s/cm^2/sr) displayed with all mice imaged on their ventral side on the same shared scale. **(f)** Same as (e) but with ssAAV8-EF1α-FLuc; same shared scale as (e). **(g)** Quantification of rAAV1 FLuc radiance from (e). Each symbol = mean signal (+/- SD) from 3 mice. Human rAAV1 is more potent ($P < 0.0001$ wk 8). **(h)** Quantification of the rAAV8 FLuc radiance from (f). Human rAAV8 is more potent ($P < 0.0001$ wk 8).

To determine whether the significant functional and sexually dimorphic hepatic expression differences were restricted to rAAV1, we repeated the same *in vivo* experiment with rAAV8. Here again, twenty-four mice (12 male, 12 female) were injected IV with 5e10 vg/mouse of ssAAV8-EF1a-FLuc produced in either platform and live-imaged weekly for FLuc expression (**Figure 4b**). The results demonstrated that our previous findings with IV administered rAAV1 were not serotype specific, as they were replicated with rAAV8 ($P < 0.05$-0.0001) (**Figure 4d**).

Discussion

Of the nearly 400 FDA-approved protein-containing therapies in use in the United States—enzymes, growth factors, interferons, hormones, blood products, vaccines, antibodies, anti-venoms, anti-toxins, immune globulins, gene therapies, cell therapies, etc.—only three (all vaccines) are produced in any insect manufacturing system (**Table S24**)[38,39]. Within the rAAV gene therapy space, the human and insect manufacturing systems are predominantly used for production. However, no public or extensive head-to-head comparison free from competitive bias has characterized final end product composition and potency from these lead manufacturing systems. Clinicians, patients and regulators need to be confident in the safety and efficacy of rAAV for gene delivery. One safety concern is the potential for immunotoxicity against insect impurities[40]. Indeed, several recent severe adverse events with fever[7,8] occurred following high dose rAAV administration with baculovirus-*Sf9* produced vector. Given the recent explosion of rAAV use--in trials for gene therapy, passive vaccines, and as a critical delivery agent in the rapidly expanding gene editing space--a thorough characterization of rAAV produced using different manufacturing methods was warranted.

Here we reported the following findings: rAAV capsids can be post-translationally modified (acetylation, methylation, phosphorylation, O-glcNAcylation, deamidation); capsid PTMs differ when produced in the baculovirus-*Sf9* and human manufacturing platforms; impurities were different in vector when produced in either platform; HCP impurities can have their own PTMs, including N-linked glycans; capsid PTMs and HCP impurities were seen across rAAV serotypes, manufacturers, and purification types; there was no difference in the packaged rAAV genome sequence in either production platform; baculovirus-*Sf9* vectors have insect and baculoviral HCP impurities and can have poorer packaging percentages than human-produced vector; both full and empty rAAV capsids have only minor structural differences when produced in either production platform; when given at the same vector genome dose, human-produced rAAVs can be more potent than baculovirus-*Sf9* vectors *in vitro* and *in vivo*; and lastly, regardless of the manufacturing platform, functional rAAV transduction is sexually dimorphic in the liver when administered IV, but not in skeletal muscle when administered IM.

It is known that human and insect cells have different capacities to post-translationally modify and fold proteins[9]. However, we were initially hesitant to speculate on the presence of PTMs on rAAV given a publication from 2006 stating that there were none[41]. We noted several key differences between this study and ours. First, they used wild-type AAV2 produced in HeLa cells with wild-type replication-competent Adenovirus-2. Modern rAAV production now produces vector in HEK293 cells and provides the adenoviral helper function from Adenovirus-5 *in trans* from plasmids[3]. Collectively, the differences in cell type (HeLa vs. HEK293), method of helper viral administration (live Ad-2 vs. Ad-5 plasmid), and type of AAV (wtAAV vs rAAV), made us question whether the AAV particles each of us assessed were comparable. Indeed, with these differences and using more sensitive LC-MS/MS instruments, we observed numerous PTMs on rAAV capsids. Additionally, there have been several recent attempts[15,42,43] to characterize rAAV vector lots, however each had limitations in either technology or scope, and called for the deeper research performed here. Our study used orthogonal methods to deeply characterize and validate each difference in a sensitive and unbiased manner.

As we designed experiments, we had to consider limitations as to which experimental parameters we could control. First, while clinical trials use Good Manufacturing Practices (GMP) grade vector, it is not possible to acquire aliquots of existing GMP lots as an external investigator, and the cost to produce even a single GMP lot renders cross comparative paired studies as performed here, prohibitive if not impossible. Thus, although we used preclinical grade vector, we ensured that it was of the highest possible purity and was identically purified for each production method. However, it is important to recognize that GMP vectors from different production methods may or may not exhibit the differences we observed.

Several technical challenges prevented us from performing desired enzymatic experiments to add/remove PTMs to intact capsids to assess the contribution to potency. For example, there are no pan-demethylase or pan-deacetylase enzymes that work on intact proteins. Similarly, deglycosidases like PNGase-F perform optimally on denatured proteins, making it difficult to assess whether capsid glycans influence potency without altering capsid structural integrity. Further, many of these modifications are in the capsid lumen, and are not accessible. One could set up a number of mutational analyses knocking out each host gene encoding each respective transferase for each PTM; however, given the number of different PTMs, there are too many host genes to knock out simultaneously without negatively affecting host cell viability.

Although we observed differences in PTMs on baculovirus-*Sf9* and human-produced vector lots by LC-MS/MS, it is important to note that PTM absence does not indicate that one was not present. Observed PTMs were substoichiometric, with the majority of identified peptides being unmodified. Further, labile modifications may be lost during sample preparation or ionization prior to detection. Quantifying PTM frequency is challenging. In many cases, PTMs are not site-localizable, which can dramatically sway accuracy of quantitative evaluations of site occupancy. Additionally, different peptides from an individual protein can differ in cleavage efficiency. Thus, the list we have reported here should not be considered exhaustive, but rather, partially complete. A requirement for inclusion in our list of observed PTMs was that the modification must be site-localizable. To ensure our spectra were correctly assigned via automated database searching, every spectrum matching to a post-translationally modified peptide was manually validated.

The field would benefit from a continued examination of the influence of production variables on vector lot composition, stability, potency and safety. These include factors such as suspension versus adherent cell culture, different purification methods, vector age, and more. For example, what effect does the use of live viruses like baculovirus (or herpes simplex virus) have during production? The initial motivation to adopt the baculovirus-*Sf9* production system stemmed from poor vector yields in adherent HEK293 cells. However, yields from new suspension-adapted HEK293 cells boost vector yields up to 1E5 vector genomes (vg)/cell[23], higher than that achieved with the baculovirus-*Sf9* system at 7E4 vg/cell[4–6]. Additional parameters that could be enhanced include improving continuous rAAV collection from suspension media[44], boosting host expression of key production factors[45], engineering other mammalian lines to safely and efficaciously produce at high yield, developing tunable cell-free methods to produce rAAV, and beyond.

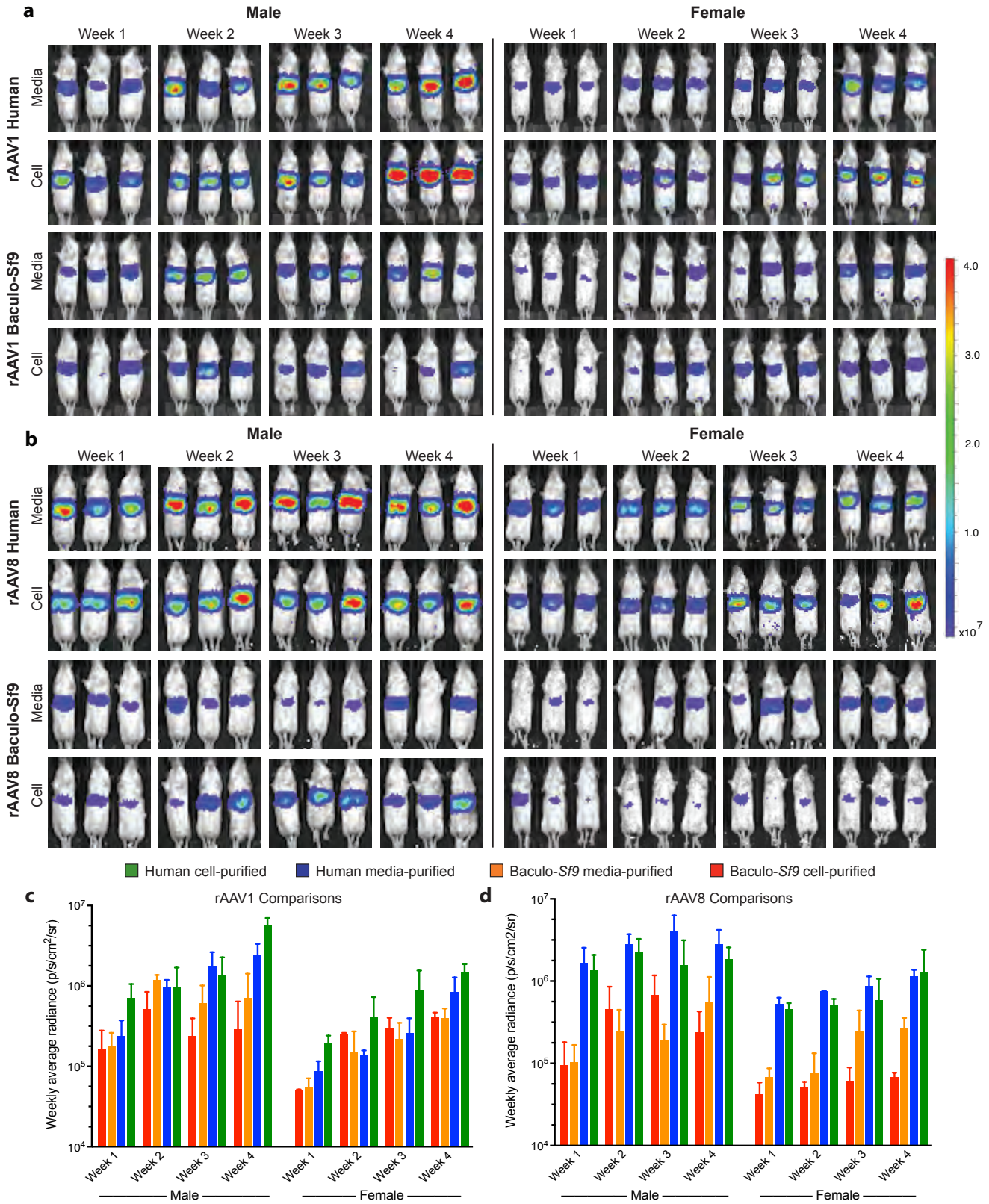

Figure 4: Functional transduction of liver tissue with rAAV is sexually dimorphic following intravenous administration *in vivo*. (a) Time course functional transduction FLuc data from human and baculo-*Sf9* produced ssAAV1-EF1α-FLuc after IV tail vein administration (5E10 vg/mouse) in age-matched male and female sibling Balb/SCID mice. Mean radiance (p/s/cm^2/sr) displayed; all mice imaged on their ventral side, same shared scale. **(b)** Same as (a) but with rAAV8; same shared scale as (a). **(c)** Quantification of (a). Human rAAV1 is more potent than baculovirus-*Sf9* rAAV1 (P < 0.05-0.0001) and males have higher functional liver transduction than females (P < 0.05-0.0001). **(d)** Quantification of (b). Human rAAV8 is also more potent (P < 0.05-0.0001) and males again have higher functional liver transduction (P < 0.05-0.0001).

Given the catalog of observed differences between the two rAAV vector manufacturing platforms characterized herein, a continued investigation into the implications of these differences for the clinical and research communities is warranted.

This article contains supporting figures and tables online.

Author Contributions

N.K.P. conceived the idea for the study. N.K.P, N.G.R., S.A.M., and A.P.M. designed the experiments. N.K.P, N.G.R., S.A.M., N.P., L.H.M., G.C., C.A., R.D.L., D.T., S.S., K.H., P.S. and A.P.M. generated reagents, protocols, performed experiments, and analyzed data. N.K.P. wrote the manuscript. N.G.R., S.A.M., N.P., L.H.M., and N.K.P. generated the figures. All authors reviewed, edited and approved the manuscript.

Acknowledgments

The authors wish to acknowledge John Perrino of the Stanford University Cell Sciences Imaging Facility and Tom Moninger of the University of Iowa Central Microscopy Research Facility for help with TEM images; Yael Rosenberg-Hasson of the Stanford Human Immune Monitoring Core for help with the Luminex assays; Parastoo Azadi of the Complex Carbohydrate Research Center at the University of Georgia for glycoproteomic help; Robert Kotin of the University of Massachusetts for the baculovirus-*Sf9* AAV2-hAADC samples; Linda Couto of The Children's Hospital of Philadelphia for the Huh7 cells; the entire staff of the University of Iowa Viral Vector Core Facility for collaborative viral productions; Bruce Conklin of the Gladstone Institute and UCSF for the human iPSC cells; the authors also wish to thank the following investigators for initial discussions: Carolyn Bertozzi and Mark Kay of Stanford University, and Joseph DeRisi of UCSF. This research was supported by grants to N.K.P. from the NIH (K01-DK107607, U01-HL145795), an American Society of Gene & Cell Therapy Career Development Grant, the Sandler Family Foundation, a Stanford University Immunity, Transplantation and Infection Young Investigator Award, and a Vincent Coates Foundation Mass Spectrometry Laboratory seed grant; grants to the University of Iowa Viral Vector Core from the NIH (P01-HL51670), the Center for Gene Therapy of Cystic Fibrosis (P30-DK54759), and the Holden Comprehensive Cancer Center (P30-CA086862); computing resources from Wynton a UCSF Shared Research Computing Cluster (https://wynton.ucsf.edu/); and funding from the Chan Zuckerberg Biohub and Cold Spring Harbor Labs; N.G.R. and S.A.M. were supported by the NIH (U01-CA207702) and HHMI, and S.A.M. was also supported by an NIH fellowship F32-GM126663; and N.P. was supported by an NIH Microbial Pathogenesis and Host Defense training grant T32-AI060537. The contents of this publication are solely the responsibility of the authors and do not necessarily represent the official views of the funding bodies, or the respective universities, institutes and organizations.

Conflicts of Interest

No corporate funding was used for this study. No authors have stock and/or equity in companies with technology related to data in this study. No authors have paid board positions, or accepted travel money, or had paid speaking engagements for companies with technology related to this study. No authors have commercial positions or affiliations related to data in this study. No authors have patents related to data in this study. Therefore, all authors declare no conflicts of interest for any aspect of the data presented in this study in its entirety.

Materials and Methods

Generation of pFB.AAV-EF1α-FLuc-WPRE-hGHpA_BAC-293 dual use transfer vector plasmid. The pAAV-EF1α-FLuc-WPRE-hGHpA transfer vector plasmid[36] (Addgene Cat#87951) was cut with *SbfI* dual-cutter just beyond each ITR to create a 4.3-kb fragment. To prepare the universal shuttle backbone, pFB.AAV-msc_bGHpA #G0202 from the University of Iowa was also cut with *SbfI* and the resultant purified backbone was ligated to the 4.3kb transfer vector fragment to create the 8.1-kb final construct. All components for insect replication (gentamicin-R and Tn7 transposition sites) and bacterial replication (ampicillin-R) are present on the dual-use backbone. Academic MTAs to Dr. Paulk at UCSF were acquired from The Salk Institute for use of the WPRE, and from the University of Iowa for the pFB.AAV-msc_bGHpA plasmid backbone. The final pFB.AAV-EF1α-FLuc-WPRE-hGHpA_BAC-293 plasmid has been deposited at Addgene (Cat#118412). Figure S1a was made with SnapGene v4.2.11; S1b was made with GraphPad Prism v8.0.1.

Plasmid transfection and Firefly luciferase expression assessment to validate pFB.AAV-EF1α-FLuc-WPRE-hGHpA_BAC-293. Each well of a 6-well plate was seeded with 500K HEK293T cells (ATCC Cat#CRL-3216). Once cells reached 80% confluency, equimolar concentrations of plasmid (custom plasmid and control plasmids) were transfected via $Ca_3(PO_4)_2$ transient transfection and media was changed after 8-hr. Cells were lysed 48-hrs later for FLuc quantitation using a Luciferase 1000 Assay System kit (Promega Cat#E4550) according to manufacturer's instructions and read on a Veritas luminometer. Experiments were performed in technical triplicate.

Generation of rAAV bacmids for baculovirus production. A custom pFB.AAV-EF1α-FLuc-WPRE-hGHpA bacmid was produced using the Bac-to-Bac production system where MAX Efficiency DH10Bac *E. coli* (Thermo Cat#10361012) contained a baculovirus shuttle vector that can recombine with a donor plasmid, pFastBac (pFB), to create an expression bacmid containing the cloned construct for eventual rAAV transfer vector production. The donor plasmid was the custom pFB.AAV-EF1α-FLuc-WPRE-hGHpA_BAC-293 construct described above. For transposition, 10-ng of pFB.AAV-EF1α-FLuc-WPRE-hGHpA_BAC-293 donor plasmid was transposed into 100-mL DH10Bac competent cells and plated on DHBac10 LB agar plates for 48-72 hours at 37^0C in a non-CO_2 incubator. Plates with colonies were kept at 4^0C thereafter until ready for use. A single large isolated transposed white colony was picked and re-streaked for isolation on another DHBac10 LB agar plate. The confirmation colony was inoculated into DHBac10 LB broth and the bacmid grown for 20-hrs in a 200-rpm shaking incubator at 37^0C. Bacmid DNA was isolated with a NucleoBond Xtra Midi EF kit (Macherey-Nagel Cat# 740.420.50), resuspended in TE, and stored in aliquots at -20^0C. The packaging bacmids for generating baculoviruses for producing different serotypes of rAAV were produced as described above, except using pFB donor plasmids encoding AAV2 Rep and the capsid of interest (pFB-AAV-Rep2/Cap8 or pFB-AAV-Rep2/Cap1) from University of Iowa.

Generation of baculoviral lots for rAAV production. For BAC-AAV-EF1α-FLuc-WPRE-hGHpA and BAC-AAV-Rep2/Cap1 or 8, $2x10^6$ *Sf9* cells (Expression Systems Cat# 94-001S) were seeded per well in a 6-well plate in protein-free ESF 921 media (Expression Systems Cat# 96-001) with no additives or antibiotics, using cells from a 3-day-old suspension culture in mid-log phase (95-100% visual viability). Cells were allowed to attach at 27^0C for 1-hr (~80% confluency). The transfection solution was prepared with 45-mg of purified bacmid in 600-mL media, and mixed with 36-mL of Cellfectin (Invitrogen Cat#10362-010) in 600-mL media, mixed and incubated at RT for 30-min. Adherent

cells were washed and then transfected with 700-mL per well of transfection solution diluted in 3-mL media. Cells were incubated for 5-hr in a 27^0C incubator in a humidity chamber. Following incubation, transfection mix was removed and 2-mL of fresh media was added per well before incubation for 5 days at 27^0C. Resultant baculovirus was harvested from the media supernatant and mixed with serum to [final] 5% for storage. Media was spun at 500xG for 5-min to pellet any cellular debris. Solution was filtered through a Millex 0.22-µm sterile syringe filter with PES membrane (EMD Millipore Cat# SLGP033RB) and aliquoted. Baculoviral titers were determined using a BackPak Baculovirus Rapid Titer kit (Clontech Cat# 631406).

Production of rAAV from baculovirus infection of *Sf9* cells for paired productions. For rAAV production, $2x10^6$ suspension *Sf9* cells/mL were seeded in 400-mL ESF 921 media in roller bottles. 24-hrs later, cells were counted for infection calculations and to ensure high viability. 100-mL of fresh media was added to each flask prior to infection. Baculoviral aliquots were thawed, resuspended, and 0.5-MOI of each baculovirus (transfer vector virus and pseudotyping virus) were added directly to the media and bottles were returned to the incubator for 72-hr at 27^0C. For production of the special empty capsid lots, the transfer vector baculovirus was omitted and only the pseudotyping baculovirus was used to ensure no transfer vector was present to package.

Production of rAAV in HEK293FT cells for paired productions. Recombinant AAV vector productions were produced in 40 15-cm plates using a $Ca_3(PO_4)_2$ transient triple transfection protocol in adherent HEK293FT cells (Thermo Fisher Cat# R70007) in DMEM + 10% FBS +1% penicillin/streptomycin. Plasmids included: pHelper (1000-mg/40 plates), pFB.AAV-EF1α-FLuc-WPRE-hGHpA_BAC-293 transfer vector plasmid (500-mg/40 plates), and a pseudotyping plasmid (pRep2/Cap8 or pRep2/Cap1; 1500-mg/40 plates). Transfection solution was incubated with cells for 16-hr at 37^0C, then the media was changed to serum-free Expi293 media (Thermo Cat#A14351) for the remaining 60-hr incubation at 37^0C in 5% CO_2. For production of the special empty capsid lots, the transfer vector plasmid was omitted and only the pHelper and pseudotyping plasmids were used to ensure no transfer vector was present to package.

Universal harvest protocol for isolating rAAV from cell lysates and media supernatant from both human and baculovirus-*Sf9* production platforms for paired productions. To isolate rAAV particles from cell lysates and media supernatant, the following protocols were followed. For cell-purified rAAV: cell pellets were lysed with a 12-min glass bead vortex, treated with 100-U/mL Benzonase (Sigma Cat# E8263-25KU) for 30-min at 37^0C followed by addition of 10% sodium deoxycholate and another 30-min 37^0C incubation to dissociate particles from membranes. Then they were iodixanol gradient-purified in OptiSeal polyallomer tubes (Beckman Cat# 362183) in a VTi-50 rotor spun at 40,000-rpm for 1-hr 50-min at 18°C in an Optima LE-80K-Beckman ultracentrifuge, further purified by MustangQ ion exchange chromatography on a peristaltic pump, and buffer exchange through an Amicon Ultra-15 centrifugal filter concentrator (Millipore Cat#UFC910096) into 1X dPBS pH 7.4 + 180-mM NaCl + 0.001% Lutrol (v/v). For media-purified rAAV: media was first put through a 100-kDa MWCO filter (Spectrum Cat#S02-E100-10N), then tangential flow filtered at 400mL/min with TMP of 4.0, then Triton-X-100 was added to 0.5% [final] and incubated in a shaking water bath at 37^0C for 1-hr, solution was then treated with 200U/l Turbonuclease (Sigma Cat#T4330-50KU) for 1-hr at 37^0C, then iodixanol gradient purified as described above, followed by MustangQ ion exchange chromatography as described above, and buffer exchanged as described above. rAAV vectors were simultaneously titered by TaqMan qPCR (on the same plate) within the hGHpA element with the following primer/probe set:

Fwd: 5'-TGTCTGACTAGGTGTCCTTCTA-3'
Rev: 5'-CTCCAGCTTGGTTCCCAATA-3'
Probe: 5'/6-FAM/AAGTTGGGAAGACAACCTGTAGGGC/IBFQ/-3'

Production of rAAV in HEK293T cells for non-paired productions. Recombinant AAV vector productions were produced using a $Ca_3(PO_4)_2$ transient triple transfection protocol in adherent HEK293T cells (ATCC Cat#CRL-3216) followed by double cesium chloride density gradient purification and dialysis as previously described[36], and resuspended in dPBS with 5% sorbitol (w/v) and 0.001% Pluronic F-68 (v/v). Plasmids included: pAd5 helper, rAAV transfer vector (ssAAV-CAG-TdTomato, Addgene #59462), and pseudotyping plasmids for each capsid of interest. rAAV vectors were titered by TaqMan qPCR within the CAG promoter with the following primer/probe set:

Fwd: 5'-GTTACTCCCACAGGTGAGC-3'
Rev: 5'-AGAAACAAGCCGTCATTAAACC-3'
Probe: 5'/FAM/CTTCTCCTCCGGGCTGTAATTAGC/BHQ-1/-3'

Two-dimensional gel electrophoresis. Protein samples for each production platform were fractionated by two-dimensional gel electrophoresis. To determine whether differences between gels resulted from differences in capsid PTMs, half of the samples were treated with a broad-spectrum lambda protein phosphatase (NEB Cat#P0753L) and PNGase-F (Promega Cat#V4831) prior to two-dimensional gel electrophoresis. 50-mg total protein from each production platform was used per preparation. Total sample volumes were adjusted to 200-µL after addition of 20-µL each of the 10X $MgCl_2$ and 10X phosphatase buffer (supplied with enzyme) per tube (regardless of enzyme treatment). 1.25-µL of enzyme was added to the phosphatase-treated samples, with the remainder being water. Samples were gently mixed and incubated for 2-hr at 30°C at 1,000-rpm. 100-mM Dithiothreitol (DTT) in water (BIO-WORLD Cat#404200001) was then added to each tube to a final concentration of 5-mM, and samples were heated at 95^0C for 5-min. Samples were cooled to 25°C before adding 5-µL of PNGase-F and incubated at 37°C overnight at 1,000 rpm. To separate proteins by their isoelectric points, samples were then loaded in equal volumes into 24 wells of an Agilent 3100 OFFGEL Fractionator using a high-resolution fractionation kit (Agilent Cat#5067-0201). Each sample, with and without enzyme treatment, was run on a separate lane of a 24 well gel strip with a linear gradient from pH 3-10 following manufacturer instructions. Runs were completed upon reaching a total of 64-kW hrs. Samples from each well were concentrated to ~30-µL with Amicon Ultra 10-KDa molecular weight cutoff spin filters (EMD Millipore Cat#UFC501008) for 2-hrs before loading into a 4-12% Bis-Tris SDS-PAGE gel (Invitrogen Cat#NP0322BOX). Gels were washed, fixed, and stained overnight with SYPRO Ruby protein gel stain (FisherSci Cat#S12000) following manufacturer instructions. Gels were then washed and imaged with a UV transilluminator.

To test whether proteases were present (in either the rAAV lots, phosphatase or PNGase-F reagents) and responsible for the banding patterns seen in Fig. S7, samples were prepared as above, but with or without pre-treatment with protease inhibitor (Roche Cat#04693159001) in combination with phosphatase treatment, PNGase-F treatment, or both. Lactoferrin was used as a positive glycoprotein control.

Subsequent Western blots on 2D-gel electrophoresis SDS-PAGE gels. Gels were transferred onto nitrocellulose membranes (Bio-Rad

Cat#1620112) with a Trans-Blot Turbo Transfer System (Bio-Rad), blocked with Odyssey Blocking Buffer (TBS) (LI-COR Cat#927-50000), blotted with rabbit anti-AAV-VP1/2/3 polyclonal antibody (ARP Cat#03-61084) at 1:200 overnight at 4^0C, then washed with PBS-T and incubated with secondary goat anti-rabbit IgG IRDye 800CW (LI-COR Cat#926-32211) at 1:10,000 for 1-hr at 25^0C. The membranes were then washed with PBS-T and visualized on a Licor Odyssey CLx Infrared Imaging System. Imaging analysis was performed using the Licor Image Studio Lite software.

Proteolytic digests of rAAV samples for LC-MS/MS. Protein preparations for paired rAAV productions were done using equal amounts of total protein (10-50 µg depending on the run). Each sample was precipitated using 4X volume of LC-grade acetone at -80^0C overnight. Precipitated protein was centrifuged at 12,500xG for 15-min at 4^0C. Supernatant was decanted and discarded and the protein pellet dried within a biosafety hood for 30-min. The pellet was resuspended in 100-µL of 0.2% Protease Max Surfactant Trypsin Enhancer (Promega Cat# V2071), 50-mM ABC, and reduced using DTT to a final concentration of 10-mM at 55^0C for 30-min. Following reduction, proteins were alkylated with 20-mM propionamide at 25^0C for 30-min. For those samples undergoing Endoglycosidase-H (Endo-H) treatment, samples were heated to 95^0C for 5-min, followed by the addition of 5-µL Endo-H reaction buffer and 5-µL Endo-H (Promega Cat#PRV4875, 2,500-U). Deglycosylation proceeded for 4-hours at 37^0C. Endo-H is a recombinant glycosidase which hydrolyses the bond connecting the two GlcNAc groups comprised in the chitobiose core, leaving a single GlcNAc covalently bound for mass spectrometry detection. 500-ng of Trypsin/Lys-C Mix (Promega Cat#V5072) was added and allowed to digest overnight for ~18-hr at 37^0C. The digest was acidified to 1% formic acid to quench protease activity. Peptides were purified on C18 MonoSpin SPE columns (GL Sciences Cat#5010-21701), and peptide pools dried to completion in a speed vac.

Liquid chromatography–mass spectrometry for non-glycosylated peptides. Peptide pools were reconstituted in 0.2% formic acid, 2% acetonitrile, and water and then injected onto a Waters M-Class UPLC. The analytical column was pulled and packed in-house using a C18 matrix (Dr. Maisch, 2.4-µM, Pur), at approximately 25-cm in length. The flow rate was 300-nL or 450-nL per minute where mobile phase A was 0.2% formic acid in water, mobile phase B was 0.2% formic acid in acetonitrile. The mass spectrometer used was an Orbitrap Fusion Tribrid (Thermo Scientific) set to acquire data in a dependent fashion using multiple fragmentation types: collision-induced dissociation (CID), higher-energy collisional dissociation (HCD), and electron-transfer dissociation (ETD). The instrument parameters used in this study were the following: CID data were generated when the precursor mass resolution was 120,000 with a *m/z* window of 400-1500, and charge states of 2+, 3+ and 4+ were sampled. The precursor automated gain control (AGC) settings were 200,000 ions and the "fastest" mode was used for MS/MS in the ion trap. The ion trap sampled the most intense precursors where the isolation window was set at 1.6-Da and the collision energy at 35. In a HCD experiment, the settings were the same as for CID except a normalized collision energy of 42 was used and fragment ions were sent to the Orbitrap for detection. Finally, in ETD/HCD triggered experiments, the precursor mass resolution was 120,000, with a *m/z* window of 400-1600, and charge states of 2-6+ were sequenced and precursor AGC target was 400,000. The instrument alternated sequencing the same precursor masses first by ETD--where the settings were a 50-ms reaction time and 200,000 reagent target--and a max ETD time of 200-ms. Fragment ions were read out in the ion trap in a centroid fashion. HCD had a collision energy of 32 and a maximum inject time of 54-ms where fragment ions were read out of the Orbitrap in a centroid fashion. The isolation window for both the fragmentation types was 1.2-Da and the data dependent acquisition exclusion settings allowed for sampling of the same precursor three times before it was placed on the exclusion list. The exclusion list was set to 10-ppm and in the ETD/HCD trigger experiment timed out after 10-sec.

Triggered liquid chromatography–mass spectrometry for glycosylated peptides. Samples were analyzed by online nanoflow LC-MS/MS using an Orbitrap Fusion Tribrid mass spectrometer (Thermo Fisher Scientific) coupled to a Dionex Ultimate 3000 HPLC (Thermo Fisher Scientific). Sample were loaded via autosampler onto a 20-µL sample loop and injected at 0.3-µL/min onto a 75-µm x 150-mm EASYSpray column (Thermo Fisher Scientific) containing 2-µm C18 beads. Columns were held at 40°C using a column heater in the EASY-Spray ionization source (Thermo Fisher Scientific). Samples were eluted at 0.3-µL/min using a 90-min gradient and 185-min instrument method. Solvent A was comprised of 0.1% formic acid in water, whereas Solvent B was 0.1% formic acid in acetonitrile. The gradient profile was as follows (min:%B) 0:3, 3:3, 93:35, 103:42, 104:98, 109:98, 110:3, 185:3. The instrument method used an MS1 resolution of 60,000 at FWHM 400-*m/z*, an AGC target of 3e5, and a mass range from 300 to 1,500-*m/z*. Dynamic exclusion was enabled with a repeat count of 3, repeat duration of 10-sec, and an exclusion duration of 10-sec. Only charge states 2-6 were selected for fragmentation. MS2s were generated at top speed for 3-sec. HCD was performed on all selected precursor masses with the following parameters: isolation window of 2-*m/z*, 28-30% collision energy, orbitrap (resolution 30,000) detection, and an AGC target of 1e4 ions. ETD was performed if: (a) the precursor mass was between 300 and 1000-*m/z*; and (b) 3 of 7 glyco-fingerprint ions (126.055, 138.055, 144.07, 168.065, 186.076, 204.086, 274.092, 292.103) were present at +/- 0.5-*m/z* and greater than 5% relative intensity. ETD parameters were as follows: calibrated charge-dependent ETD times, 2e5 reagent target, and precursor AGC target 1e4.

Mass spectra data analysis. MS/MS data were analyzed using both Preview and Byonic v2.10.5 software (ProteinMetrics). Data were first analyzed in Preview to validate calibration and trypsin/chymotrypsin digestion efficiency. Initial Byonic analyses used a concatenated FASTA file containing the AAV sequences, host proteomes (*Spodoptera frugiperda*, *Homo sapiens*, and *Autographa californica multiple nuclepolyhedrovirus* (baculovirus)) and other likely contaminants and impurities to verify sample purity. Once sample complexity was determined, a second round of Byonic analyses were completed using a targeted FASTA file containing the AAV sequence of interest and likely impurities to identify peptides and potential PTMs. Data were searched at 10-12 ppm mass tolerances for precursors (depending on the run), with 10-12 ppm or 0.1-0.4 Da fragment mass tolerances for HCD and ETD fragmentation, respectively. The algorithm allowed up to two missed cleavages per peptide and semi-specific, N-ragged tryptic digestion. These data were validated at a 1% false discovery rate using standard reverse-decoy techniques[46]. The resulting identified peptide spectral matches and assigned proteins were then exported for further analysis and validated using custom tools to provide visualization and statistical characterization. All PTM mass spectra were also manually validated.

***De novo* glycan identification.** Glycopeptide sequences were determined by *de novo* manual interpretation of HCD and ETD mass spectra. Extracted chromatograms were generated for all MS2s containing 204.0867 ions (+/- 10-ppm), and all spectra containing this ion were analyzed. HCD spectra were used to approximate glycan structures, and ETD spectra were used to define peptide sequence and

site-localize modifications. GalNAc and GlcNAc were distinguished by their defined HexNAc fingerprints, as described previously[47].

Animals. Adult SCID-Balb/cJ mice (CBySmn.CB17-Prkdcscid/J) of each sex were purchased from The Jackson Laboratories (Cat#1803) for imaging studies. The Institutional Animal Care & Use Committees of UCSF and Stanford University approved all mouse procedures.

***In vitro* transduction analysis by Firefly luciferase quantitation.** Five cell types were assessed: immortalized human HEK293T cells (ATCC Cat# CRL-3216), immortalized mouse C2C12 myoblasts (ATCC Cat#CRL-1772), immortalized human Huh7 hepatocarcinoma cells (gift of Linda Couto), primary Hs27 human fetal foreskin fibroblasts (ATCC Cat#CRL-1634) all maintained in DMEM (Gibco Cat# 11995065) supplemented with 10% FBS and 1% antibiotic/antimycotic; and primary human iPSC cells (Coriell Cat# GM25256) derived from the skin biopsy of a healthy 30-year-old Japanese male which were maintained with the following modifications from a recent protocol[48]: used Matrigel growth factor reduced basement membrane matrix (Corning Cat#354230) in feeder-free media conditions (Gibco Essential 8 Flex Media Cat# A2858501) with a seeding density of 35K/cm^2. Accutase (STEMCELL Technologies Cat# 07920) and 10-M RHO/ROCK pathway inhibitor Y-276932 (STEMCELL Technologies Cat# 72304) were used to dissociate iPSCs to single cells during passaging. In all cell types, 1-hr prior to transduction at 80% confluency, media was changed, then 80K cells/condition were transduced with ssAAV1-EF1α-FLuc-WPRE-hGHpA vectors diluted in dPBS at MOI 80K. The following day, media was replaced to remove vector that did not transduce and media was not changed again. FLuc levels were measured 3-days post-AAV administration using a Luciferase 1000 Assay System (Promega Cat#E4550) per manufacturer instructions and read on a Veritas luminometer at: 100-µL luciferin injection, 2-sec delay, 10-sec measure. Experiments were performed in technical triplicate and corrected for background by subtracting signal from PBS-diluent negative control wells. Figure 3a was generated with GraphPad Prism v8.0.1.

Human tissue. We obtained anonymized human induced pluripotent stem cells derived from normal controls enrolled in ongoing, CHR-approved studies for basic research purposes by the human gamete, embryo and stem cell research committee to Dr. Bruce Conklin under the UCSF IRB#10-02521 "Induced Pluripotent Stem Cells for Genetic Research". The iPS cells were originally derived from a 30-year-old Japanese male who signed a consent form approving the donation of iPS cells to the public stem cell bank Coriell (Cat# GM25256).

Mixed titration/empty spike-in transduction analysis *in vitro*. Human HEK293T cells were maintained as described above. One hour prior to transduction at 80% confluency, media was changed, and 60K cells were transduced with varying ratios of full:empty ssAAV1-EF1α-FLuc-WPRE-hGHpA vectors produced by either platform and diluted in dPBS (only cell-purified vector was used). The total capsid content was kept constant at MOI 30K, while the ratio of full:empty varied: 30K:0K (0% empty), 27K:3K (10% empty), 15K:15K (50% empty), 3K:27K (90% empty), 0K:30K (100% empty). The following day, media was replaced to remove non-transducing vector and the media was not changed again. FLuc levels were measured 3-days post-AAV administration using a Luciferase 1000 Assay System kit (Promega Cat#E4550) per manufacturer's instructions and read on a Veritas luminometer with settings: 100-µL luciferin injection, 2-sec delay, 10-sec measure. Experiments were performed in 6 biological replicates and corrected for background by subtracting the signal from the PBS-diluent negative control wells. Figures 3c,d were generated with GraphPad Prism v8.0.1.

Live *in vivo* transduction analysis by Firefly luciferase imaging and quantitation in mice. All mice having received either intravenous normodynamic lateral tail vein injections or intramuscular (*tibialis anterior*) injections of 5E10 vg/mouse of ssAAV-EF1α-FLuc-WPRE-hGHpA (both rAAV8 and rAAV1) were imaged non-invasively every 7-days on a Xenogen IVIS Spectrum imaging system (Caliper Life Sciences). D-luciferin substrate (Biosynth Cat#L-8220) was administered at 120-mg/kg in saline by intraperitoneal injection with a 1-cc insulin syringe. Images were acquired 10-min after luciferin administration under inhalation isoflurane anesthesia. Living Image v4.5 software was used for image analysis and average radiance was quantified in p/s/cm^2/sr. All mice in each experiment are shown on the same non-individualized radiance scale to enable accurate comparisons of bioluminescent intensity.

Silver staining. Viral lots were TaqMan qPCR titered (as described above) and 1E10 vg worth of vector was mixed with 5-µL of 4X NuPage LDS Buffer (Invitrogen Cat#NP0007) and 2-µL of 10X NuPage Reducing Agent (Invitrogen Cat#NP0009) and boiled for 8-min. Boiled samples were loaded into 4-12% 1-mm 12-well Bis-Tris NuPage gels (Invitrogen Cat#NP0322PK2) along with 0.5-µL of Benchmark Unstained Protein Ladder (Invitrogen Cat#10747-012) and run in 1X NuPAGE MES buffer (Invitrogen Cat#NP0002) supplemented with 500-µL NuPage Antioxidant (Invitrogen Cat#NP0005) at 100-V for 2.8-hrs. Gels were rinsed in 18 MΩ water, fixed and stained using a SilverQuest Staining Kit (Invitrogen Cat#LC6070) according to manufacturer's instructions.

Luminex cytokine assay. Primary human fetal foreskin fibroblasts (ATCC Cat#CRL-1634) were maintained in DMEM (Gibco Cat#11995065) supplemented with 10% FBS and 1% antibiotic/antimycotic and seeded at 12K per well in a 96 well plate. 24-hrs following seeding, at 24K confirmed cells/well (control wells for each condition were lifted, counted and verified for viability), media was changed and allowed to sit for 1-hr prior to transduction with four rAAV lots of ssAAV8-EF1a-Fluc-WPRE produced by either platform and purified from either cell lysate or media supernatant (as described above) at an MOI of 100K in a total final media volume of 200-µL. No further media changes or washes occurred until media harvest at 24-hrs following rAAV addition. Controls included 'media only' wells (no cells or rAAV), and 'media + cells' wells (no rAAV) for background normalization calculations. Media was harvested from each well, spun at 350-rcf for 5-min at 4^{0}C to pellet any cells, and media supernatants were then aliquoted in four protein LoBind polypropylene tubes (Eppendorf Cat#022431081) per well for storage at -80^{0}C until use in the assay. Conditions were set up in biological triplicate and run in technical duplicate. The assay was performed at the Human Immune Monitoring Center at Stanford University. A custom human 63-plex kit was purchased from eBiosciences and used according to the manufacturer's recommendations with modifications described below. Briefly: beads were added to a 96-well plate and washed in a Biotek ELx405 washer. Thawed samples were added to the plate containing the mixed antibody-linked beads and incubated at 25°C for 1-hr followed by overnight incubation at 4°C with shaking. Cold and 25°C incubation steps were performed on an orbital shaker at 500-600 rpm. Following the overnight incubation, plates were washed in a Biotek ELx405 washer and then biotinylated detection antibody added for 75-min at 25°C with shaking. The plate was washed as above and streptavidin-PE was added. After incubation for 30-min at 25°C, a wash was performed as above and reading buffer was added to each well. Each sample was measured in duplicate. Plates were read using a Luminex 200 instrument with a lower

bound of 50 beads per sample per cytokine. Custom assay control beads by Radix Biosolutions were added to all wells. Data were normalized to controls with no AAV added during production (plain host cells cultured for either 24-hr or 48-hr) and averaged across all biological replicates. Data were visualized in R Studio.

Next-generation sequencing of packaged rAAV genomes using Fast-Seq. Total packaged gDNA was extracted from 1E11 full rAAV particles for each lot of rAAV8 and rAAV1 sequenced. AAV libraries were prepared following a novel Tn5 tagmentation-based protocol called Fast-Seq, developed for this study and described in detail separately on protocols.io[32]. The following indexed adapters compatible with Illumina were obtained from IDT:

Index 1 (i7):
CAAGCAGAAGACGGCATACGAGAT*NNNNNNNNNNNN*GTCTCGTGGGCTCGG

Index 2 (i5):
AATGATACGGCGACCACCGAGATCTACAC*NNNNNNNNNNNN*TCGTCGGCAGCGTC

bold = P5/P7 adapter sequence
italics = unique 12-bp barcode index
underline = primer for mosaic ends added during tagmentation

Each adapter contained a 12-nucleotide unique barcode for identifying samples after multiplexing. Indexes used for each sample are listed in **Table S18**. The resulting library was diluted to 10-pM in 600-µL of HT1 hybridization buffer (Illumina Nextera XT kit Cat#FC-131-1024) and 10-µL was loaded onto a 300-cycle MiSeq Nano v2 flow cell (Illumina Cat#MS-102-2002) for paired-end 2 x 75-bp sequencing. Resultant reads were demultiplexed using Illumina's bcl2fastq v2.19.0.316. Data were returned in fastq format and filtered using Trimmomatic[49] to remove adapter sequences, low quality reads (PHRED score <30, or length <50-bp), unmapped and unpaired reads. Trimmed reads were then aligned to the rAAV transfer vector plasmid reference sequence with BWA v0.7.17[50], using the mem algorithm. Alignments were saved as BAM files, which were then used to generate VCF files using GATK Haplotype Caller algorithm[51]. SNPs and indels identified in VCF files were filtered using BCFtools filter algorithm, with a 15X depth threshold and a 90% allele fraction requirement. A consensus sequence was generated using BCFtools consensus algorithm[52]. Alignment and fragment distribution statistics were obtained with Picard tools[53]. Coverage spanned 100% of the rAAV transfer vector genome reference sequence. Figure 3b was generated with ggplot. Figure S12b was generated with the ViennaRNA Web Services structure prediction software for DNA available at http://rna.tbi.univie.ac.at.

Capsid protein thermal stability. Purified rAAV capsids of various serotypes produced by each manufacturing platform were compared for their denaturing thermal stability. 10-µL of undiluted rAAV of each lot was loaded into a high sensitivity capillary (Nanotemper Cat#PR-C006) and run on a Nanotemper Prometheus NT.48 nanoDSF instrument. Thermal denaturation programs were run with a 1ºC/min thermal ramp from 30ºC to 95ºC with fluorescent detection at 330 and 350 nm. Data were analyzed with PR.ThermControl software v2.1.5 to determine the temperatures for T_{onset} and T_m. Figures 1m, S8 and S9k were made with GraphPad Prism v8.0.1.

Negative staining and TEM imaging. Grids were glow discharged in the presence of argon gas for 20-sec in a Denton Desktop Turbo III vacuum system and then covered with 5 to 12-µL of rAAV and allowed to adsorb to either a 300-mesh copper or 400-mesh carbon grid with Formvar and carbon coatings (Cat# FCF300-CU) for 3-min. The AAV was washed off by touching the grid, sample side down, to two drops of ddH_2O (18-MΩ). 1-2% uranyl acetate in ddH_2O (18-MΩ) was then dripped through a 0.2-µm mesh syringe filter over the grid allowing the third drop to remain on the grid for 1-min before most of the stain was wicked away with filter paper and allowed to dry. Grids were observed on either a JEOL JEM-1400 or JEOL JEM-1230 transmission electron microscope at 120-kV and photos were taken using Gatan Orius digital cameras (either 2K-x-2K or 4K-x-4K). Packaging percentage determinations from TEM images were measured in ImageJ v2.0.0-rc-43/1.52b[54].

False-colored structural capsid PTM mapping. The rAAV8 PTMs shown in Figure 1 were mapped onto the PDB AAV8 capsid structure 3RA8[16] using Pymol v1.7.6.0. The rAAV1 PTMs shown in Figure S9 were mapped onto the PDB AAV1 capsid structure 3NG9[55]. Exterior capsid views have all chains represented, while internal cross-section views have chains surrounding a cylinder at the 5-fold symmetry axis removed exposing the interior capsid lumen with fogging cued to enable depth perception of the interior. Online UbPred software (http://www.ubpred.org) was used to predict the possible ubiquitination sites on AAV1 and AAV8 capsid proteins[19]. The output of the analysis is the prediction of the lysine residues important for ubiquitination within the indicated AAV serotype capsid sequence. There were 11 lysines on rAAV1 VP3: K258, K459, K491, K493, K508, K528, K533, K545, K567, K666 and K707. There were 8 lysines on rAAV8 VP3: K259, K333, K510, K530, K547, K569, K668 and K709.

Cryo-EM data acquisition and image processing. Purified rAAV8 samples (human-produced empty and full, baculovirus-*Sf9* produced empty and full) were applied to Lacey carbon Quantifoil grids (EMS Cat# Q225CR-06) and flash frozen. Images were collected using an FEI Titan Krios G3i Cryo Transmission Electron Microscope operating at 300-kV with a Gatan K2 Summit detector and GIF using a 20-eV slit width. Movies were collected in counting mode with the automated imaging software EPU and a pixel size of 1.07 Å. 30 frames were collected in a 6-sec exposure with a per frame dose rate of 2.2 $e^-/Å^2$ for a total dose of ~66 $e^-/Å^2$. A total of 1,647 movies were collected for human-produced rAAV8 and 396 movies were collected for baculovirus-*Sf9* produced rAAV8. Movies were drift-corrected using MotionCor2[56]. All image processing was performed using cisTEM[57]. No symmetry was applied for initial 2D classification and icosahedral symmetry was applied for 3D classification and the final reconstruction. The previous crystal structure determined for rAAV8 (PDB 3RA8) was used as an initial starting point for all models. Residues were manually fit in Coot[58] and refined against the cryo-EM maps using Phenix.real_space_refine[59]. These 4 new structures are being deposited in PDB and EMDB.

Signal peptide determination. Putative ER signal peptides of the AAV VP1 polypeptide were found using LocSig Database software (http://genome.unmc.edu/LocSigDB)[30]. Only signals within the first 100 amino acid residues of VP1 from the N-terminal end were assessed.

Gene ontology analysis on host cell protein impurities. The cumulative HCP impurities from all vector lots analyzed by LC-MS/MS (human impurities observed in human vector preparations; human impurities observed in baculovirus-*Sf9* vector preparations; *Spodoptera frugiperda* impurities observed in baculovirus-*Sf9* vector preparations; baculoviral impurities observed in baculovirus-*Sf9* vector preparations) were ranked by PSM. For human impurities, those with a PSM greater than 3 were

analyzed by gene ontology functional enrichment analysis using g:Profiler[60], version e94_eg41_p11_9f195a1, with g:SCS multiple testing correction method applying significance threshold of 0.05 and an ordered query to generate Figure S11a. Only impurities from *Homo sapiens* could be assessed with these bioinformatic tools as both *Spodoptera frugiperda* and *Autographa californica multiple nuclepolyhedrovirus* (NPVAC, baculovirus) were not supported organisms. Gene ontologies for *Sf9* and *NPVAC* were assessed manually using UniProtKB.

Statistics. Statistical analyses were conducted with Prism v8 software. Experimental differences for Figures 3a,c,d and S1 were evaluated using a one-way ANOVA with Tukey's correction for multiple comparisons assuming equal variance. Experimental differences for Figures 3e-h, 4, and S13 were evaluated using a two-way ANOVA with Tukey's correction for multiple comparisons assuming equal variance. P values <0.05 were considered statistically significant. * $P \leq 0.05$, ** $P \leq 0.01$, *** $P \leq 0.001$, **** $P \leq 0.0001$.

References

1. Nakai, H. *et al.* Extrachromosomal recombinant adeno-associated virus vector genomes are primarily responsible for stable liver transduction in vivo. *J. Virol.* **75**, 6969–6976 (2001).
2. Alexander, I. E., Russell, D. W., Spence, A. M. & Miller, A. D. Effects of gamma irradiation on the transduction of dividing and nondividing cells in brain and muscle of rats by adeno-associated virus vectors. *Hum. Gene Ther.* **7**, 841–850 (1996).
3. Grimm, D., Kern, A., Rittner, K. & Kleinschmidt, J. A. Novel tools for production and purification of recombinant adenoassociated virus vectors. *Hum. Gene Ther.* **9**, 2745–2760 (1998).
4. Urabe, M., Ding, C. & Kotin, R. M. Insect cells as a factory to produce adeno-associated virus type 2 vectors. *Hum. Gene Ther.* **13**, 1935–1943 (2002).
5. Smith, R. H., Levy, J. R. & Kotin, R. M. A simplified baculovirus-AAV expression vector system coupled with one-step affinity purification yields high-titer rAAV stocks from insect cells. *Mol. Ther.* **17**, 1888–1896 (2009).
6. Aslanidi, G., Lamb, K. & Zolotukhin, S. An inducible system for highly efficient production of recombinant adeno-associated virus (rAAV) vectors in insect *Sf9* cells. *Proceedings of the National Academy of Sciences* **106**, 5059–5064 (2009).
7. https://investors.biomarin.com/2019-01-07-BioMarin-Highlights-Key-Milestones-for-2019-at-37th-Annual-J-P-Morgan-Healthcare-Conference-in-San-Francisco.
8. https://www.pfizer.com/news/press-release/press-release-detail/sangamo_and_pfizer_announce_phase_1_2_interim_data_for_investigational_hemophilia_a_gene_therapy.
9. Varki, A. *Essentials of Glycobiology*. (Cold Spring Harbor Laboratory Press, 2017).
10. van Ree, R. Carbohydrate epitopes and their relevance for the diagnosis and treatment of allergic diseases. *Int. Arch. Allergy Immunol.* **129**, 189–197 (2002).
11. European Medicines Agency Assessment Report, Glybera. (2012). Available at: https://www.ema.europa.eu/en/documents/assessment-report/glybera-epar-public-assessment-report_en.pdf. (Accessed: 16th April 2019)
12. Padron, E. *et al.* Structure of adeno-associated virus type 4. *J. Virol.* **79**, 5047–5058 (2005).
13. Kronenberg, S., Böttcher, B., von der Lieth, C. W., Bleker, S. & Kleinschmidt, J. A. A conformational change in the adeno-associated virus type 2 capsid leads to the exposure of hidden VP1 N termini. *J. Virol.* **79**, 5296–5303 (2005).
14. Sonntag, F., Bleker, S., Leuchs, B., Fischer, R. & Kleinschmidt, J. A. Adeno-associated virus type 2 capsids with externalized VP1/VP2 trafficking domains are generated prior to passage through the cytoplasm and are maintained until uncoating occurs in the nucleus. *J. Virol.* **80**, 11040–11054 (2006).
15. Giles, A. R. *et al.* Deamidation of Amino Acids on the Surface of Adeno-Associated Virus Capsids Leads to Charge Heterogeneity and Altered Vector Function. *Mol. Ther.* **26**, 2848-2862 (2018).
16. Nam, H. J. *et al.* Structure of adeno-associated virus serotype 8, a gene therapy vector. *J. Virol.* **81**, 12260–12271 (2007).
17. Akache, B. *et al.* The 37/67-kilodalton laminin receptor is a receptor for adeno-associated virus serotypes 8, 2, 3, and 9. *J. Virol.* **80**, 9831–9836 (2006).
18. Gurda, B. L. *et al.* Mapping a neutralizing epitope onto the capsid of adeno-associated virus serotype 8. *J. Virol.* **86**, 7739–7751 (2012).
19. Radivojac, P. *et al.* Identification, analysis, and prediction of protein ubiquitination sites. *Proteins* **78**, 365–380 (2010).
20. Becerra, S. P., Koczot, F., Fabisch, P. & Rose, J. A. Synthesis of adeno-associated virus structural proteins requires both alternative mRNA splicing and alternative initiations from a single transcript. *J. Virol.* **62**, 2745–2754 (1988).
21. Galibert, L. *et al.* Origins of truncated supplementary capsid proteins in rAAV8 vectors produced with the baculovirus system. *PLoS One* **13**, e0207414 (2018).
22. Gaudet, D. et al. Efficacy and long-term safety of alipogene tiparvovec (AAV1-LPLS447X) gene therapy for lipoprotein lipase deficiency: an open-label trial. Gene Ther. 20, 361–369 (2013).
23. Grieger, J. C., Soltys, S. M. & Samulski, R. J. Production of Recombinant Adeno-associated Virus Vectors Using Suspension HEK293 Cells and Continuous Harvest of Vector From the Culture Media for GMP FIX and FLT1 Clinical Vector. *Mol. Ther.* **24**, 287–297 (2016).
24. Venkatakrishnan, B. *et al.* Structure and dynamics of adeno-associated virus serotype 1 VP1-unique N-terminal domain and its role in capsid trafficking. *J. Virol.* **87**, 4974–4984 (2013).
25. Ui, N. Conformational studies on proteins by isoelectric focusing. *Ann. N. Y. Acad. Sci.* **209**, 198–209 (1973).
26. Wistuba, A., Kern, A., Weger, S., Grimm, D. & Kleinschmidt, J. A. Subcellular compartmentalization of adeno-associated virus type 2 assembly. *J. Virol.* **71**, 1341–1352 (1997).
27. Tse, L. V. *et al.* Structure-guided evolution of antigenically distinct adeno-associated virus variants for immune evasion. *Proc. Natl. Acad. Sci. U. S. A.* **114**, E4812–E4821 (2017).
28. Gurda, B. L. *et al.* Capsid antibodies to different adeno-associated virus serotypes bind common regions. *J. Virol.* **87**, 9111–9124 (2013).
29. Tseng, Y.-S. *et al.* Adeno-associated virus serotype 1 (AAV1)- and AAV5-antibody complex structures reveal evolutionary commonalities in parvovirus antigenic reactivity. *J. Virol.* **89**, 1794–1808 (2015).

30. King, B. R. & Guda, C. ngLOC: an n-gram-based Bayesian method for estimating the subcellular proteomes of eukaryotes. *Genome Biol.* **8**, R68 (2007).

31. Forte, G. M., Pool, M. R. & Stirling, C. J. N-terminal acetylation inhibits protein targeting to the endoplasmic reticulum. *PLoS Biol.* **9**, e1001073 (2011).

32. Maynard, L. *et al.* Fast-Seq, a universal method for rapid and inexpensive genomic validation of rAAV vectors in preclinical settings v1 doi:10.17504/protocols.io.utzewp6.

33. Deal, C. E. & Balazs, A. B. Vectored antibody gene delivery for the prevention or treatment of HIV infection. *Curr. Opin. HIV AIDS* **10**, 190–197 (2015).

34. Paulk, N. K. *et al.* Bioengineered Viral Platform for Intramuscular Passive Vaccine Delivery to Human Skeletal Muscle. *Mol Ther Methods Clin Dev* **10**, 144–155 (2018).

35. Vercauteren, K. *et al.* Superior In vivo Transduction of Human Hepatocytes Using Engineered AAV3 Capsid. *Mol. Ther.* **24**, 1042–1049 (2016).

36. Paulk, N. K. *et al.* Bioengineered AAV Capsids with Combined High Human Liver Transduction In Vivo and Unique Humoral Seroreactivity. *Mol. Ther.* **26**, 289–303 (2018).

37. Liu, Q. *et al.* Neutralizing antibodies against AAV2, AAV5 and AAV8 in healthy and HIV-1-infected subjects in China: implications for gene therapy using AAV vectors. *Gene Ther.* **21**, 732–738 (2014).

38. Vaccines, Blood & Biologics. Available at: https://www.fda.gov/BiologicsBloodVaccines/default.htm.

39. Walsh, G. Biopharmaceutical benchmarks 2014. *Nat. Biotechnol.* **32**, 992–1000 (2014).

40. Ghaderi, D., Zhang, M., Hurtado-Ziola, N. & Varki, A. Production platforms for biotherapeutic glycoproteins. Occurrence, impact, and challenges of non-human sialylation. *Biotechnol. Genet. Eng. Rev.* **28**, 147–175 (2012).

41. Murray, S. *et al.* Characterization of the capsid protein glycosylation of adeno-associated virus type 2 by high-resolution mass spectrometry. *J. Virol.* **80**, 6171–6176 (2006).

42. Kondratov, O. *et al.* Direct Head-to-Head Evaluation of Recombinant Adeno-associated Viral Vectors Manufactured in Human versus Insect Cells. *Mol. Ther.* **25**, 2661–2675 (2017).

43. Dong, B. *et al.* Proteomics analysis of co-purifying cellular proteins associated with rAAV vectors. *PLoS One* **9**, e86453 (2014).

44. Benskey, M. J., Sandoval, I. M. & Manfredsson, F. P. Continuous Collection of Adeno-Associated Virus from Producer Cell Medium Significantly Increases Total Viral Yield. *Hum. Gene Ther. Methods* **27**, 32–45 (2016).

45. Rodrigues, A. F., Carrondo, M. J., Alves, P. M. & Coroadinha, A. S. Cellular targets for improved manufacturing of virus-based biopharmaceuticals in animal cells. *Trends Biotechnol.* **32**, 602–607 (2014).

46. Elias, J. E. & Gygi, S. P. Target-decoy search strategy for increased confidence in large-scale protein identifications by mass spectrometry. *Nat. Methods* **4**, 207–214 (2007).

47. Malaker, S. A. *et al.* Identification of Glycopeptides as Posttranslationally Modified Neoantigens in Leukemia. *Cancer Immunol Res* (2017). doi:10.1158/2326-6066.CIR-16-0280.

48. Libby, A. R. *et al.* Spatiotemporal mosaic self-patterning of pluripotent stem cells using CRISPR interference. *Elife* **7**, (2018).

49. Bolger, A. M., Lohse, M. & Usadel, B. Trimmomatic: a flexible trimmer for Illumina sequence data. *Bioinformatics* **30**, 2114–2120 (2014).

50. Li, H. & Durbin, R. Fast and accurate short read alignment with Burrows-Wheeler transform. *Bioinformatics* **25**, 1754–1760 (2009).

51. McKenna, A. *et al.* The Genome Analysis Toolkit: a MapReduce framework for analyzing next-generation DNA sequencing data. *Genome Res.* **20**, 1297–1303 (2010).

52. Danecek, P. & McCarthy, S. A. BCFtools/csq: haplotype-aware variant consequences. *Bioinformatics* **33**, 2037–2039 (2017).

53. Picard Tools - By Broad Institute. Available at: https://broadinstitute.github.io/picard/.

54. Rueden, C. T. *et al.* ImageJ2: ImageJ for the next generation of scientific image data. *BMC Bioinformatics* **18**, 529 (2017).

55. Miller, E. B. *et al.* Production, purification and preliminary X-ray crystallographic studies of adeno-associated virus serotype 1. *Acta Crystallogr. Sect. F Struct. Biol. Cryst. Commun.* **62**, 1271–1274 (2006).

56. Zheng, S., Palovcak, E., Armache, J.-P., Cheng, Y. & Agard, D. Anisotropic Correction of Beam-induced Motion for Improved Single-particle Electron Cryo-microscopy. *bioRxiv* 061960 (2016). doi:10.1101/061960.

57. Grant, T., Rohou, A. & Grigorieff, N. cisTEM, user-friendly software for single-particle image processing. *Elife* **7**, (2018).

58. Emsley, P., Lohkamp, B., Scott, W. G. & Cowtan, K. Features and development of Coot. *Acta Crystallogr. D Biol. Crystallogr.* **66**, 486–501 (2010).

59. Afonine PV, Headd JJ, Terwilliger TC, Adams PD. Phenix.real_space_refine. *Computational Crystallography Newsletter* **4**, 43–44 (2013).

60. Reimand, J. *et al.* g:Profiler—a web server for functional interpretation of gene lists (2016 update). *Nucleic Acids Research* **44**, W83–W89 (2016).

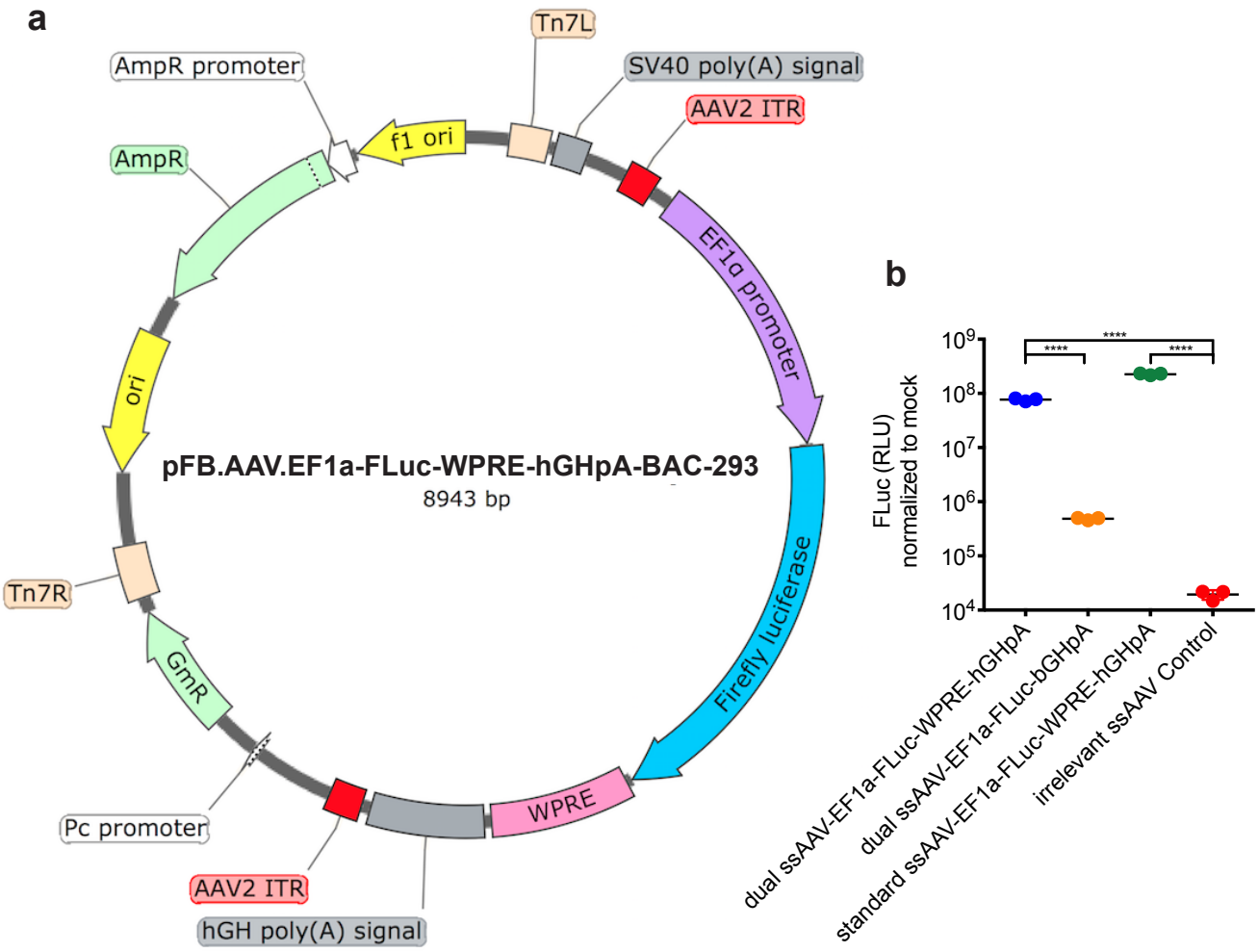

Supplemental Figure 1. Custom dual-use plasmid pFB.AAV-EF1α-FLuc-WPRE-hGHpA-BAC-293. (a) The plasmid was designed to have the necessary backbone components for use in both transient transfection into human HEK293 cells, as well as to produce live baculovirus. This ensured that the rAAV transfer vector sequence was identical between the two production platforms. Using this plasmid, each platform will produce ssAAV with an EF1α promoter driving expression of Firefly luciferase, followed by a WPRE to improve expression, and a standard hGHpA signal embedded between AAV2 ITRs. Within the backbone, two sets of important elements were included: AmpR expression components for growth in ampicillin-containing bacterial cultures for amplifying the plasmid itself; as well as gentamicin expression components and Tn7 transposition sites to allow for replication and transposition in insect cells during baculovirus production. The EF1α promoter was chosen as it is a strong ubiquitous non-tissue specific promoter that expresses well in a variety of cells/tissues both in vitro and in vivo to allow for maximal utility in the lab when making comparisons between species of interest and experimental conditions. Firefly luciferase was chosen as the reporter gene as it is easily detectable both in vitro and in vivo with highly sensitive commercial kits and common live bioluminescent imaging modalities in all tissues. WPRE inclusion enabled better expression detection, even in tissues/cells with traditionally low rAAV transduction frequencies. **(b)** FLuc expression data comparing the standard parental plasmid (only usable in the human production method) to the two dual test constructs with and without the WPRE demonstrating that the WPRE element is needed to achieve robust expression to enable comparative expression studies.

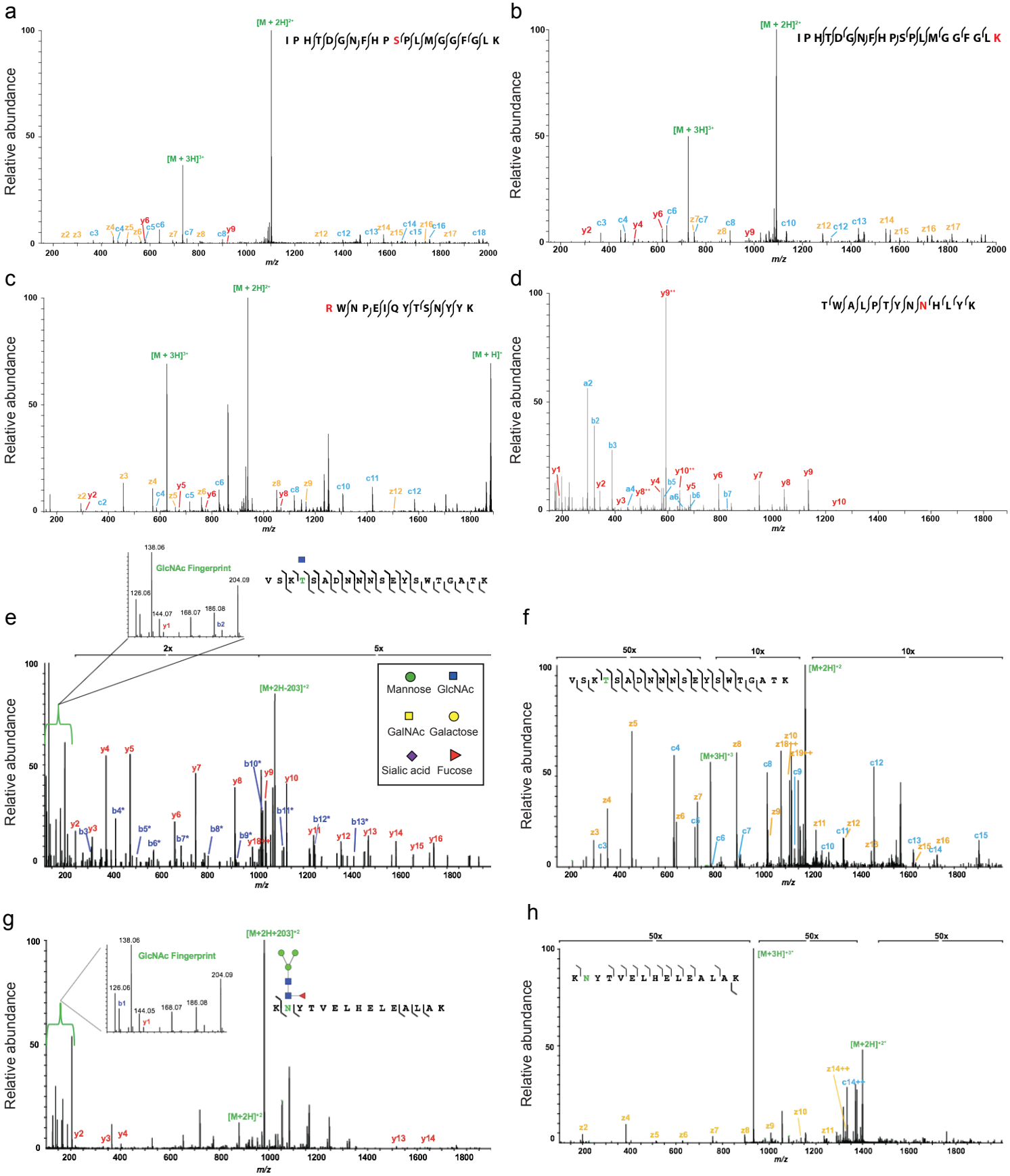

Supplemental Figure 2: Example spectra for PTMs observed on rAAV capsids and HCP impurities. (a) Example of a MS/MS fragmentation spectrum of a typical phosphorylated rAAV peptide sequence at the serine residue highlighted in red. **(b)** Example of a MS/MS fragmentation spectrum of a typical acetylated rAAV peptide sequence at the lysine residue highlighted in red. **(c)** Example of a MS/MS fragmentation spectrum of a typical methylated rAAV peptide sequence at the arginine residue highlighted in red. **(d)** Example of a MS/MS fragmentation spectrum of a typical deamidated rAAV peptide sequence at the asparagine residue highlighted in red. **(e)** Example of a typical HCD mass spectrum of a O-GlcNAcylated rAAV peptide at the initial threonine residue highlighted in green. Fragment ions that define the complete amino acid sequence are labeled as b and y. Those that have lost the O-GlcNAc moiety are labeled with an asterisk. **(f)** The associated ETD mass spectrum for (e). **(g)** Example of a typical HCD mass spectrum of an N-glycosylated *Sf9* HCP impurity peptide from ferritin with a N-GlcNAc2-Fuc-Man3 glycoform at the highlighted asparagine residue in green. Branching patterns were predicted based on known glycan structures along with sequential neutral losses from the mass spectra. **(h)** The associated ETD mass spectrum for (g).

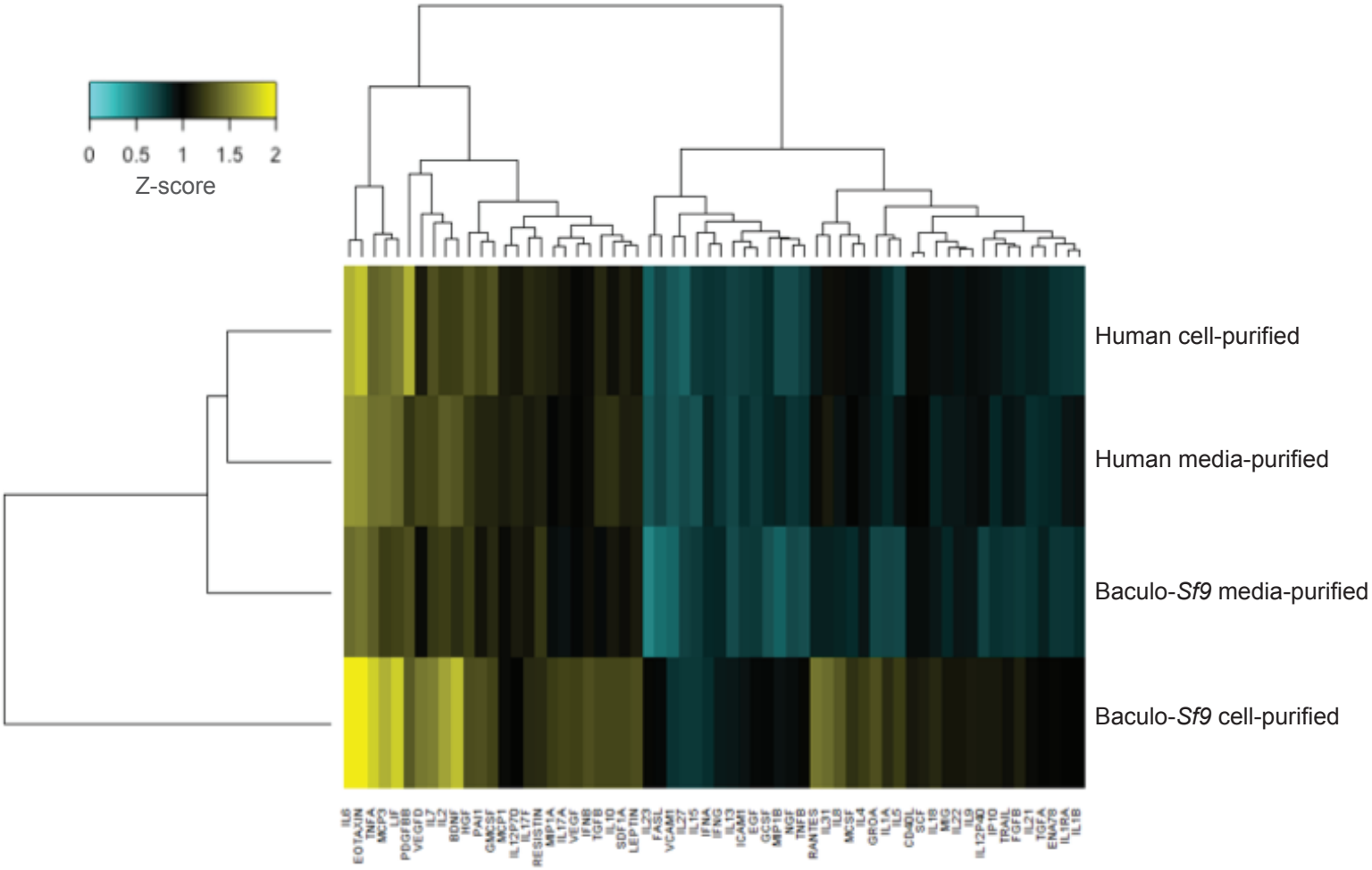

Supplemental Figure 3: Cytokine/chemokine responses of primary human fibroblasts in response to rAAV transduction by different vector lot sources. A heat map shows the results of a quantitative human 63-plex Luminex assay measured across four rAAV8 samples at 24 hours post-transduction. Heatmap cells are colored according to the normalized fold change Z score. The cluster-gram shows hierarchical clustering of virus lots based on similarity.

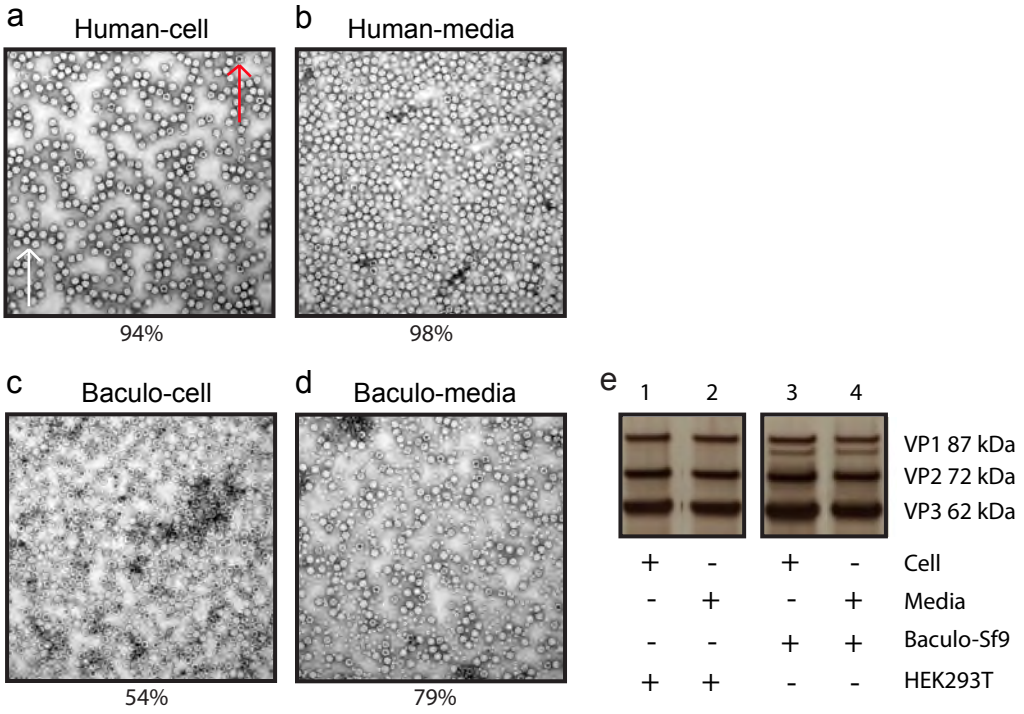

Supplemental Figure 4: Comparative proteomic profiles of repeat rAAV8 vector lots manufactured with human and second-generation baculovirus-Sf9 production platforms. (a) Negative staining and TEM imaging of human rAAV8 cell purified vector (Lot 3098, pair with b). White arrow denotes a full capsid, red arrow denotes an empty capsid, for reference for panels a-d (in all cases, the percent of full capsids containing a genome denoted below the representative TEM image above). **(b)** Negative staining and TEM imaging of human rAAV8 media purified vector (Lot 3099, pair with a). **(c)** Negative staining and TEM imaging of baculo-Sf9 rAAV8 cell purified vector (Lot 3101, pair with d). **(d)** Negative staining and TEM imaging of baculo-Sf9 rAAV8 media purified vector (Lot 3103, pair with c). **(e)** Silver stain of capsid VP protein species present in vector lots from a-d. Denoted below whether capsids were purified from cell lysates or media supernatants, and which production platform was used for vector manufacturing.

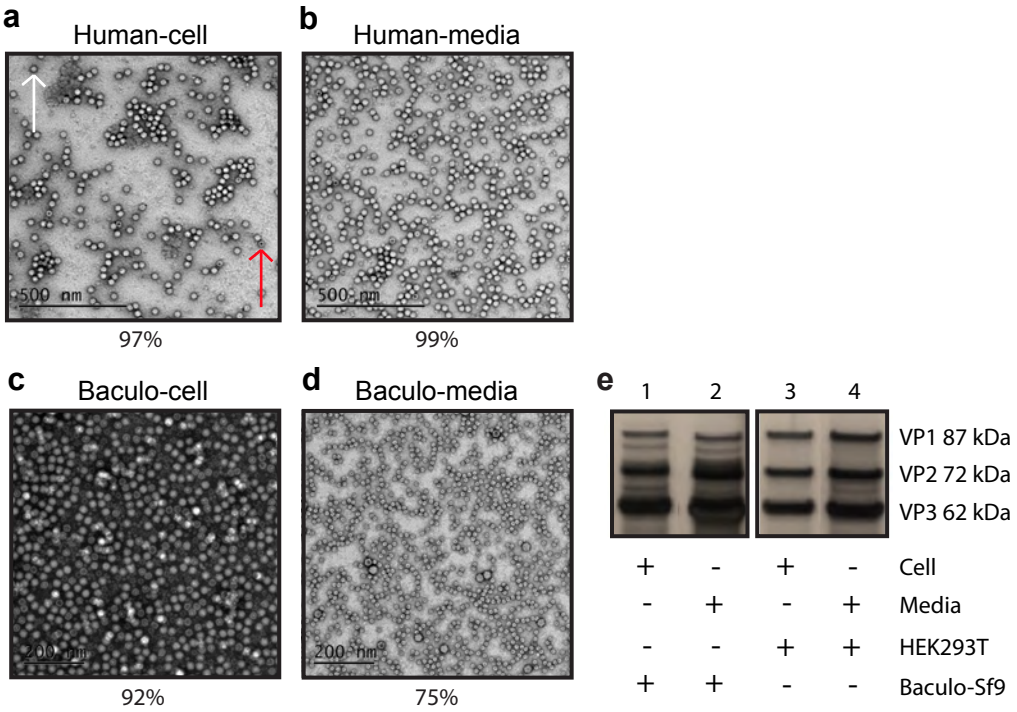

Supplemental Figure 5: Comparative proteomic profiles of repeat rAAV8 vector lots manufactured with human and first-generation baculovirus-Sf9 production platforms. (a) Negative staining and TEM imaging of human rAAV8 cell-purified vector (pair with b). White arrow denotes a full capsid, red arrow denotes an empty capsid, for reference for panels a-d (in all cases, the percent of full capsids containing a genome denoted below the representative TEM image above). **(b)** Negative staining and TEM imaging of human rAAV8 media-purified vector (pair with a). **(c)** Negative staining and TEM imaging of baculo-*Sf9* rAAV8 cell-purified vector (pair with d). **(d)** Negative staining and TEM imaging of baculo-*Sf9* rAAV8 media-purified vector (pair with c). **(e)** Silver stain of capsid VP protein species present in vector lots from a-d. Denoted below whether capsids were purified from cell lysates or media supernatants, and which production platform was used for vector manufacturing. The truncated VP species with the baculo-*Sf9* vector are particularly prominent.

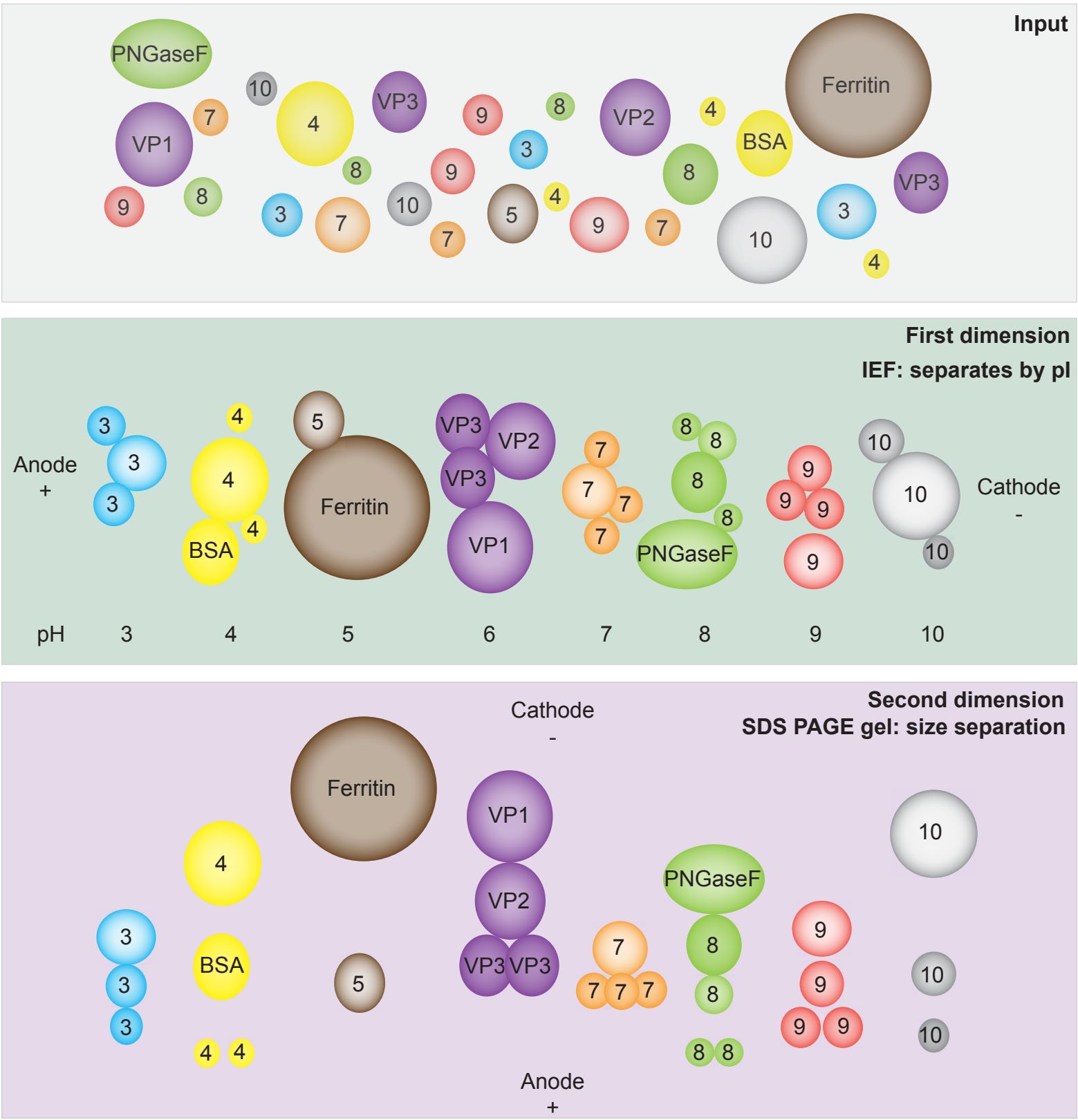

Supplemental Figure 6: Schematic of 2D-gel electrophoresis process. Vector lot samples composed of rAAV capsid proteins, host cell protein impurities and any process contaminants were loaded into precast pH gradient gel strips and run in the presence of current such that proteins migrate to the well where their isoelectric point (pI) matches the pH in the well. Once done migrating "in gel" in the first dimension, samples in each well are removed via pipet and loaded on their own lane on a standard SDS PAGE gel to separate by size in the second dimension. Running "in gel" rather than "in solution" creates bands rather than the more traditional dots.

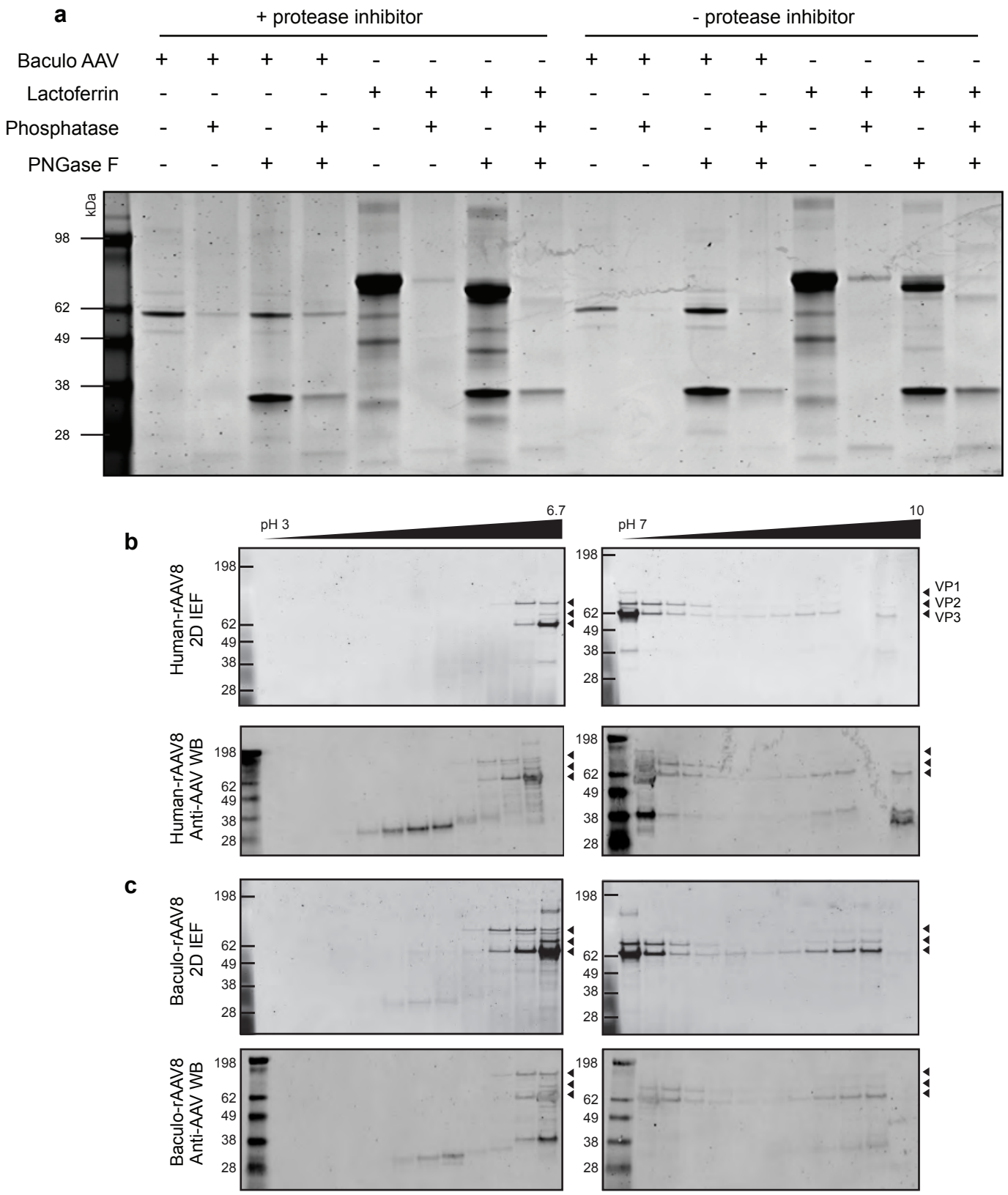

Supplemental Figure 7: 2D-gel electrophoresis control +/- protease inhibitor to confirm the lack of host protease activity. **(a)** An rAAV8 sample produced with the baculo-*Sf9* platform was subjected to standard in-gel 2D-gel electrophoresis with and without pretreatment with protease inhibitors to assess the potential for host protease action being responsible for banding patterns seen in Figure 1k,l. Experimental samples and controls: baculo-rAAV8 (VP1 87 kDa, VP2 72 kDa, VP3 62 kDa); lactoferrin (80 kDa); lambda protein phosphatase (25 kDa); PNGase F (34.8 kDa). **(b)** 2D gel images from human-produced rAAV8 from Figure 1k with corresponding anti-AAV VP1/VP2/VP3 western blot beneath. **(c)** 2D gel images from baculo-*Sf9* produced rAAV8 from Figure 1l with corresponding anti-AAV VP1/VP2/VP3 western blot beneath.

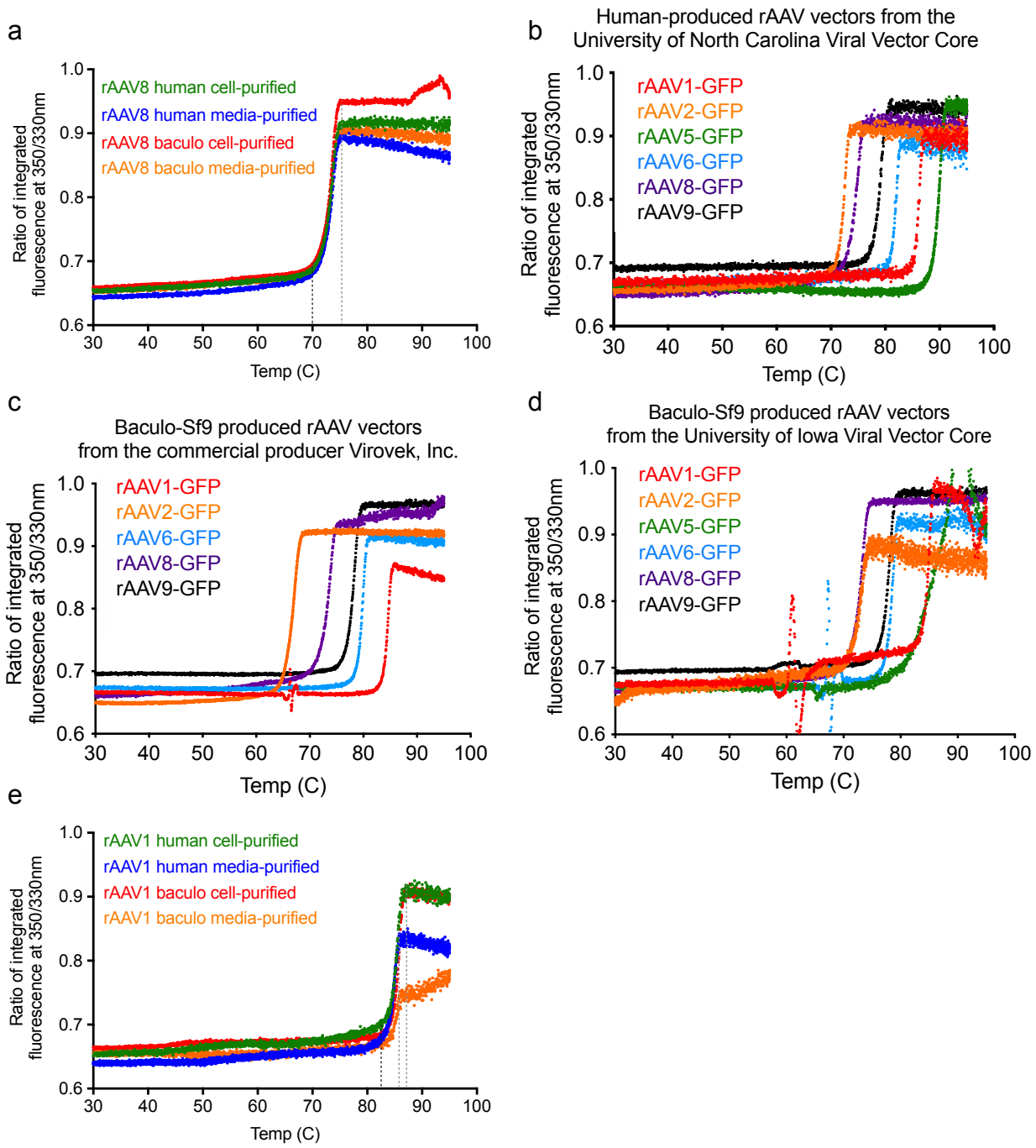

Supplemental Figure 8: Thermal capsid melt curves to predict capsid stability. (a) Full thermal capsid protein melt curves for rAAV8 vectors from 30-95C, rather than the cropped temperature curves shown in Figure 1m. Melt curve initiation is shown with a dashed black line, and final Tm is shown with a dashed grey line. No difference was seen for rAAV8 vectors produced in either manufacturing platform or purification source. **(b)** Thermal capsid melt curves for commonly used rAAV serotypes produced using transient transfection of human HEK293 cells at the UNC Viral Vector Core facility. All vectors contain the same CMV-GFP transfer cassette. The same legend color was used for panels b-d: rAAV1 (red), rAAV2 (orange), rAAV5 (green), rAAV6 (blue), rAAV8 (purple), and rAAV9 (black). **(c)** Thermal capsid melt curves for commonly used rAAV serotypes produced using live baculoviral infection of suspension *Sf9* cells at the commercial supplier Virovek, Inc. All vectors contain the same CMV-GFP transfer cassette. The aberration in signal from rAAV1 seen at 66C is common when capsids aggregate and/or when other protein contaminants are present. **(d)** Thermal capsid melt curves for commonly used rAAV serotypes produced using live baculoviral infection of suspension *Sf9* cells at the University of Iowa Viral Vector Core facility. All vectors contain the same CMV-GFP transfer cassette. Similar to the signal seen with Virovek baculoviral preparations, rAAV1 and rAAV6 had aberrant signal due to aggregation and/or contaminants. **(e)** Full thermal capsid protein melt curves for rAAV1 vectors from 30-95C, rather than the cropped temperature curves shown in Figure S9k. Melt curve initiation is shown with a dashed black line, and final Tm is shown with dashed grey lines. No difference was seen for rAAV1 vectors produced in either manufacturing platform.

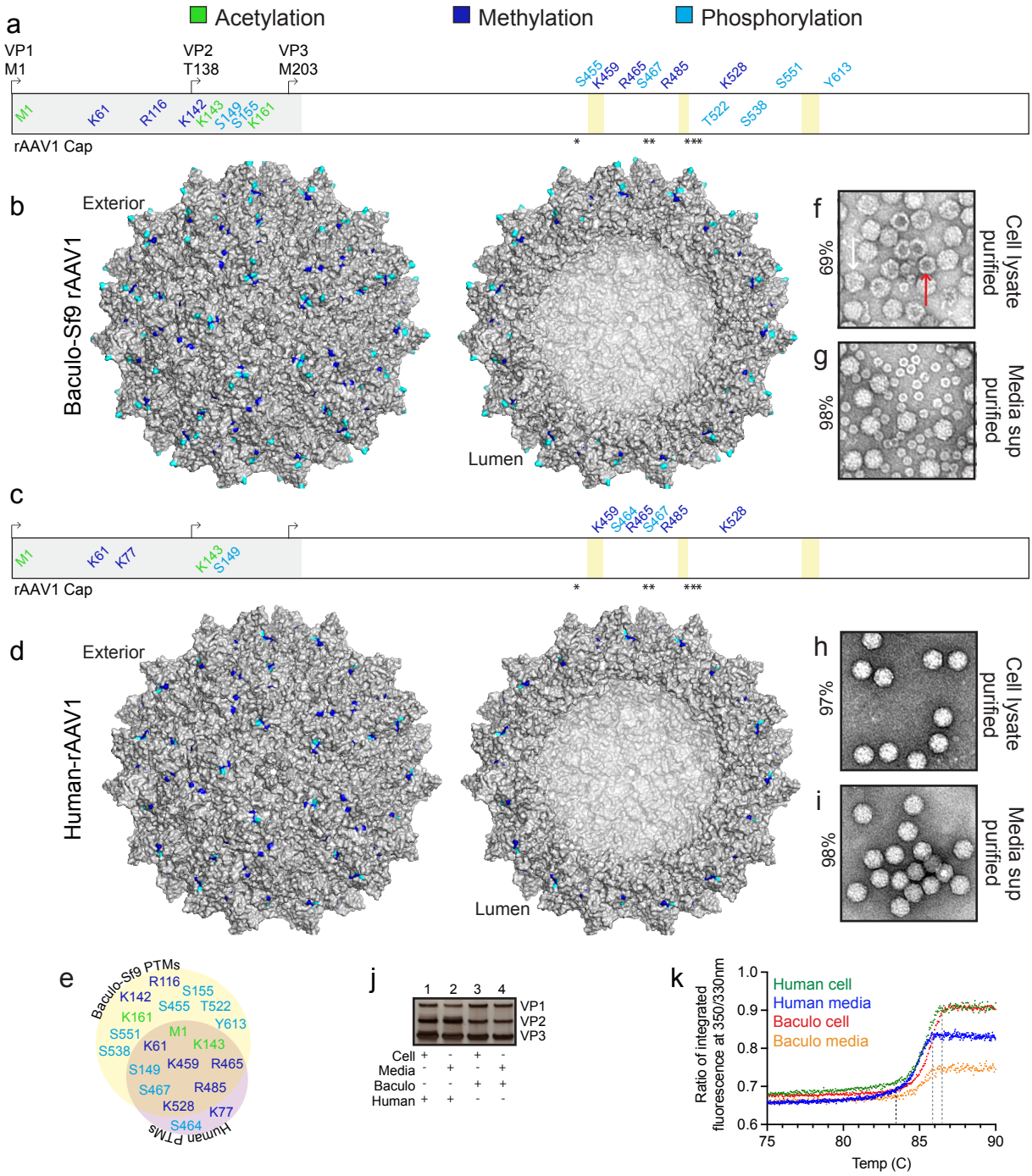

Supplemental Figure 9: AAV1 vector preparations manufactured with the human and baculovirus-*Sf9* production platforms exhibit differential PTM profiles. (a) PTM identities and residue positions along the length of the rAAV1 polypeptide from the N to C-terminus in baculo-*Sf9* vector. PTMs colored by type (acetylation = green, methylation = blue, phosphorylation = cyan). Residues above the sequence are externally facing on the capsid. Residues below are lumenal or buried. Residues within the grey box from residues 1-217 represent the disordered region of AAV1 yet to be crystallized. The six residues involved in sialic acid primary receptor binding (N447, S472, V473, N500, T502, and W503) are noted with an asterix. The three capsid motifs with known high antigenicity are denoted with yellow boxes: (456-AQNK-459), (492-TKTDNNNS-499), and (588-STD-PATGDVH-597). **(b)** Cumulative capsid PTMs observed from all baculo-*Sf9* rAAV1 lots, purified from both cell lysates and media. Color code as in (a). **(c)** Same as (a) but with human-produced rAAV1. **(d)** Same as (b) but with human rAAV1. **(e)** Shared and unique capsid PTMs for rAAV1 produced in the baculo-*Sf9* (yellow) and human systems (purple). Color code as in (a). **(f)** Negative staining and TEM imaging of baculo-*Sf9* rAAV1 cell-purified vector. White arrow denotes a full capsid, red arrow denotes an empty capsid, for reference for panels f-i (percent full capsids noted to the left). **(g)** Same as (f) but media-purified vector. **(h)** Same as (f) but with human rAAV1 cell-purified vector. **(i)** Same as (h) but with media-purified vector. **(j)** Silver stain of capsid VP species present in vector lots from panels f-i. **(k)** Thermal capsid melt curves for rAAV1 vectors shown from 75-90C, full melt curves from 30-95C are in Figure S8e. Tm initiation = dashed black line; final Tm = dashed grey line.

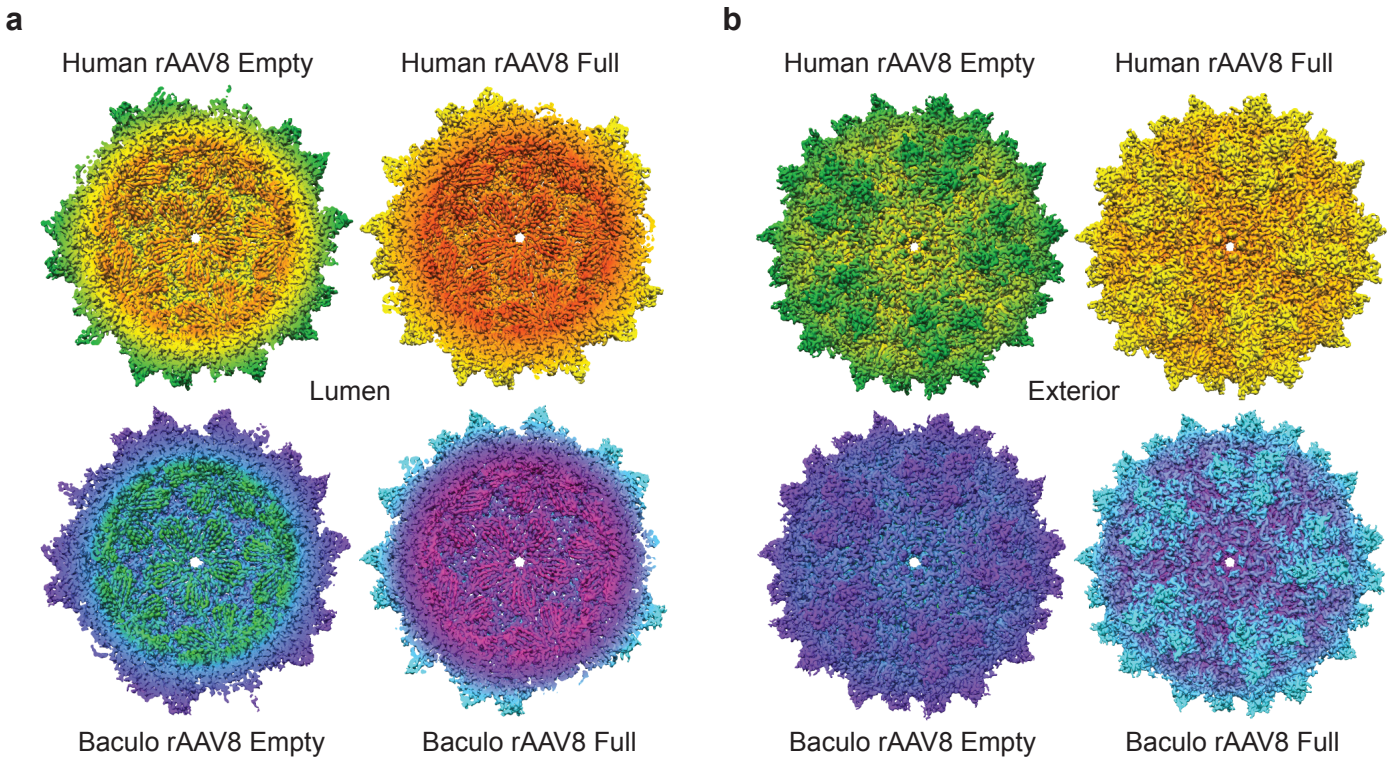

Supplemental Figure 10: Additional cryo-EM structural data from the four new rAAV8 structures of full and empty capsids from baculovirus-*Sf9* and human-produced vectors. (a) Lumenal cutaway capsid views centered on the interior base of the capsid cylinder pore of four new rAAV8 structures determined by cryo-EM. Vectors from each manufacturing platform, as well as empty and full capsids are shown. Human empty capsids are colored in orange, yellow, green; human full capsids are red, orange, yellow; baculo-*Sf9* empty capsids are green, blue, purple; and baculo-*Sf9* full capsids are pink, purple, cyan. **(b)** Exterior capsid views centered on the capsid cylinder pore of the four rAAV8 structures determined by cryo-EM. Same color scheme as in (a).

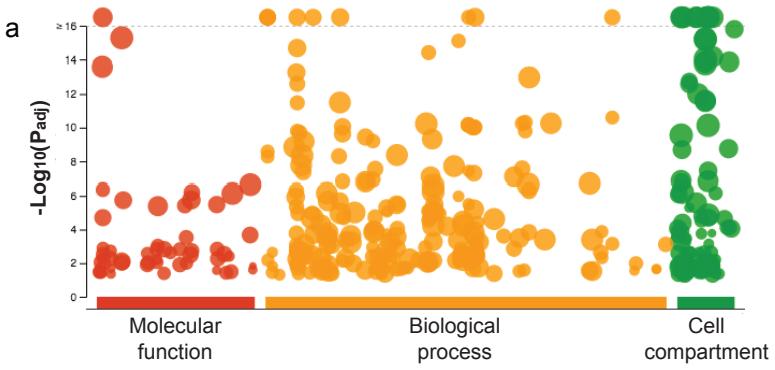

b

	H.sapiens	***S.frugiperda***	***NPVAC* (Baculovirus)**
Molecular function	Nucleic acid binding Protein binding	Endopeptidase activity Protein binding	Structural Polyhedra liberation
Biological process	RNA processing	Proteolysis Response to unfolded protein	Capsid formation Viral escape
Cell compartment	Nucleus Cytosol	Proteasome Nucleus/cytosol	Viron

Supplemental Figure 11: Cumulative comparative HCP impurity analysis. (a) Gene ontology analysis for human HCP impurities from human produced vector preparations. Only impurities from *Homo sapiens* could be assessed with these bioinformatic tools as both *Spodoptera frugiperda* and *Autographa californica multiple nuclepolyhedrovirus* (NPVAC, baculovirus) were not supported organisms. Gene ontologies for *Sf9* and NPVAC were assessed manually using UniProtKB. **(b)** Comparative gene ontology analysis for the most common HCP impurities from each host type: *H.sapiens*, *S.frugiperda* and NPVAC (baculovirus).

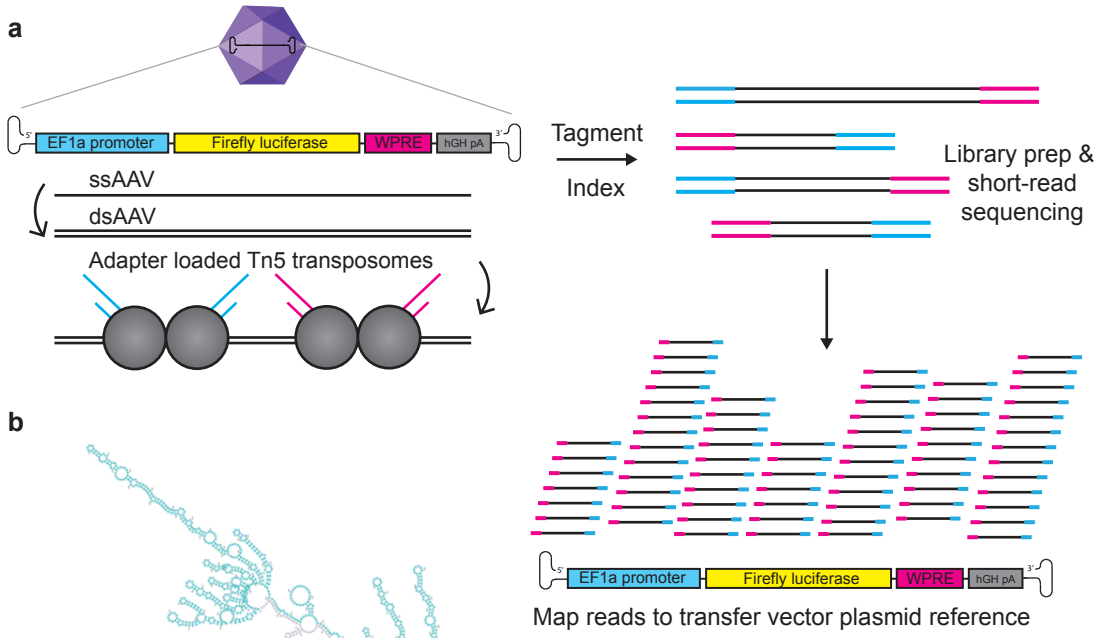

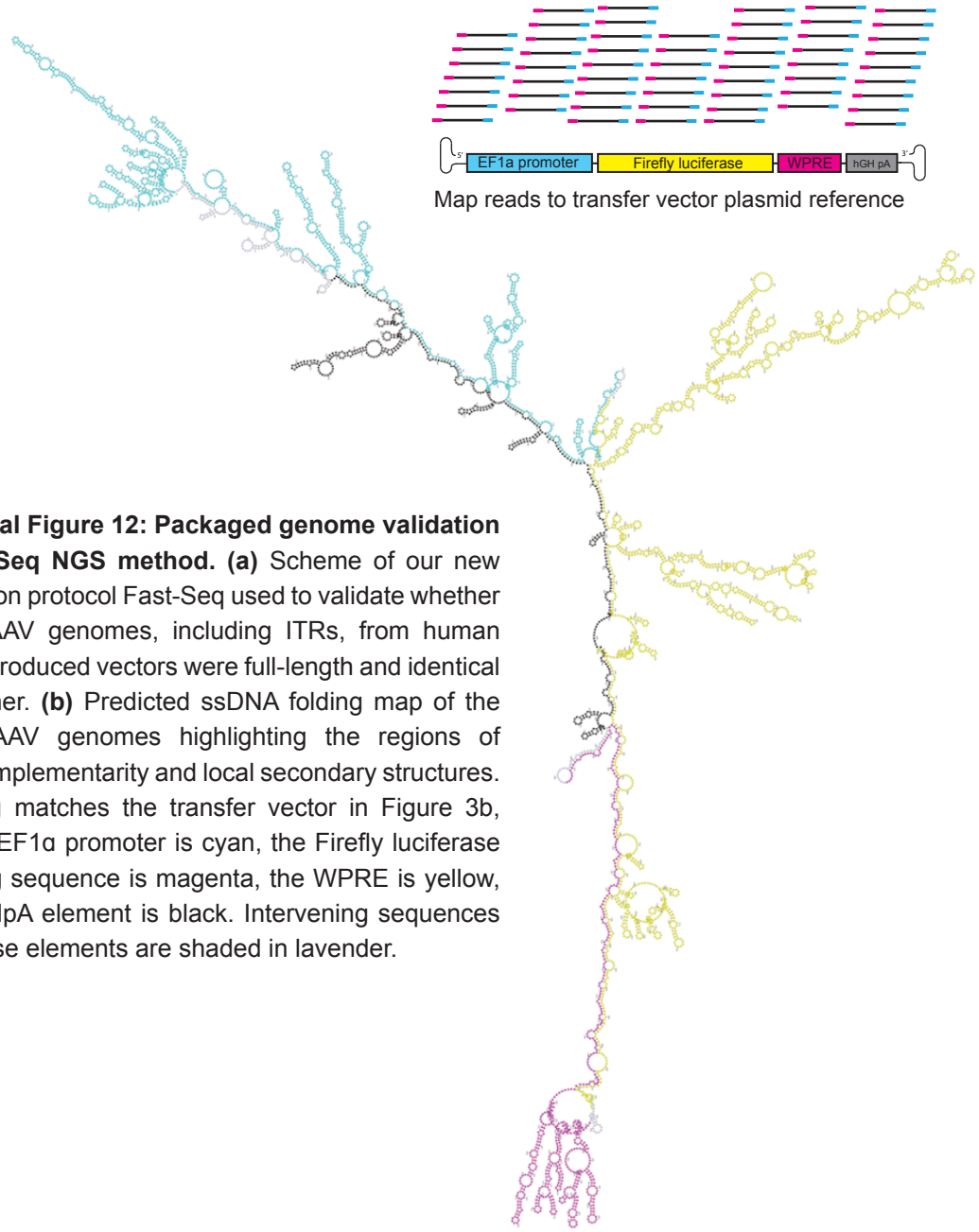

Supplemental Figure 12: Packaged genome validation using Fast-Seq NGS method. (a) Scheme of our new NGS validation protocol Fast-Seq used to validate whether packaged rAAV genomes, including ITRs, from human and baculo-produced vectors were full-length and identical to one another. **(b)** Predicted ssDNA folding map of the packaged rAAV genomes highlighting the regions of predicted complementarity and local secondary structures. Color coding matches the transfer vector in Figure 3b, wherein the EF1α promoter is cyan, the Firefly luciferase cDNA coding sequence is magenta, the WPRE is yellow, and the hGHpA element is black. Intervening sequences between these elements are shaded in lavender.

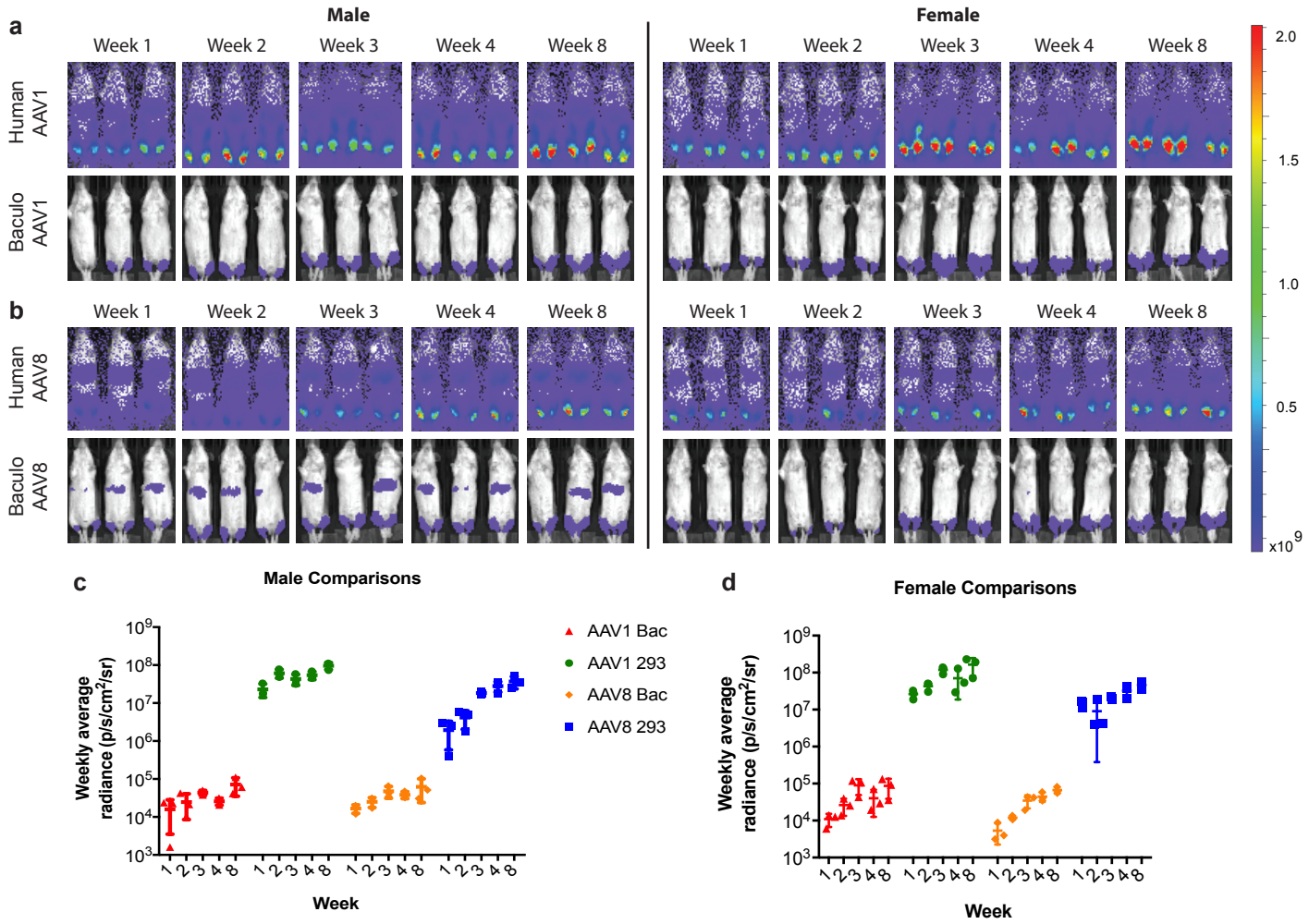

Supplemental Figure 13: Additional in vivo data from Figure 3. (a) Time course functional transduction FLuc expression from human and baculo-*Sf9* produced ssAAV1-EF1α-FLuc after IM administration (5E10 vg/mouse) in age-matched male and female sibling Balb/SCID mice. Mean radiance (p/s/cm2/sr) is displayed with all mice imaged on their ventral side on the same, shared scale. Image is shown highly blown out to enable seeing the low level of comparative expression in the baculo-treated mice (when compared to Figure 3e). **(b)** Time course functional transduction FLuc expression from human and baculo-*Sf9* produced ssAAV8-EF1α-FLuc after IM administration (5E10 vg/mouse) in age-matched male and female sibling Balb/SCID mice. Mean radiance (p/s/cm2/sr) is displayed with all mice imaged on their ventral side on the same, shared scale. Image is shown highly blown out to enable seeing the low level of comparative expression in the baculo-treated mice (when compared to Figure 3f). **(c)** Alternative representation to Figure 3g,h, now putting all serotypes on one graph and focusing on the differences in male mice. Each symbol represents the mean signal (+/- SD) from 3 mice. **(d)** Alternative representation to Figure 3g,h, now putting all serotypes on one graph and focusing on the differences in female mice. Same color legend as (b). Each symbol represents the mean signal (+/- SD) from 3 mice.

SUPPLEMENTAL TABLES

Supplemental Table 1. All HCP impurities present in human and baculovirus-*Sf9* preparations of rAAV8. All HCP impurities identified by LC-MS/MS for rAAV8 from both cell lysate and media-purified vector preparations. Excluded from the list are common process contaminants that occur in routine sample preparation (human keratin, trypsin, etc.), and impurities with mutations/aberrations such that they didn't appear in the main search library. Searches were conducted against the complete proteomes of *Homo sapiens*, *Spodoptera frugiperda*, *Autographa californica multiple nuclepolyhedrovirus* (baculovirus), *Adeno-associated virus* serotype 8, and common process contaminants (BSA from media, etc.). PSM = peptide spectral match.

[Table is an attached excel file].

rAAV	Source	Produced in	Cell or media	Purification	Titer (vg/mL)	Lot #
AAV8-EF1α-FLuc	UIowa	HEK293	Cell	I-MQ	1.10E+13	AAV3242
			Media	S-TFF-I-MQ	2.60E+13	AAV3243
		Baculo-*Sf9*	Cell	I-MQ	8.70E+13	AAV3244
			Media	S-TFF-I-MQ	3.30E+12	AAV3245

Supplemental Table 2. Viral specifications for the rAAV8 vector lots used in Figure 1. A single transfer vector plasmid lot (Figure S1) was used to produce vector in each system. Human rAAV vector lots were produced via the standard 3-plasmid transient transfection system in HEK293(FT) cells. Baculo-*Sf9* rAAV vector lots were produced via the second-generation baculovirus-infected *Sf9* cell system. All vector lots were produced with AAV2 *Rep* and AAV2 ITRs with single-stranded genome configurations. Abbreviations: I = iodixanol gradient; MQ = MustangQ column; TFF = tangential flow filtration; S = 100-kDa MWCO filter.

rAAV	Source	Produced in	Cell or media	Purification	Titer (vg/mL)	Lot #
AAV8-EF1α-FLuc	UIowa	HEK293	Cell	I-MQ	2.80E+12	AAV3098
			Media	S-TFF-I-MQ	6.00E+12	AAV3099
		Baculo-*Sf9*	Cell	I-MQ	3.50E+13	AAV3101
			Media	S-TFF-I-MQ	1.00E+12	AAV3103

Supplemental Table 3. Viral specifications for the rAAV8 vector lots used in Figure S4. A single transfer vector plasmid lot (Figure S1) was used to produce vector in each system. Human rAAV vector lots were produced via the standard 3-plasmid transient transfection system in HEK293(FT) cells. Baculo-*Sf9* rAAV vector lots were produced via the second-generation baculovirus-infected *Sf9* cell system. All vector lots were produced with AAV2 *Rep* and AAV2 ITRs with single-stranded genome configurations. Abbreviations: I = iodixanol gradient; MQ = MustangQ column; TFF = tangential flow filtration; S = 100-kDa MWCO filter.

rAAV	Source	Produced in	Cell or media	Purification	Titer (vg/mL)	Lot #
AAV8-EF1α-FLuc	UIowa	HEK293	Cell	I-MQ	4.80E+11	AAV3062
			Media	S-TFF-I-MQ	7.20E+12	AAV3060
		Baculo-*Sf9*	Cell	I-MQ	1.50E+13	AAV3061
			Media	S-TFF-I-MQ	1.80E+12	AAV3059

Supplemental Table 4. Viral specifications for the rAAV8 vector lots used in Figure S5. A single transfer vector plasmid lot (Figure S1) was used to produce vector in each system. Human rAAV vector lots were produced via the standard 3-plasmid transient transfection system in HEK293(FT) cells. Baculo-*Sf9* rAAV vector lots were produced via the first-generation baculovirus-infected *Sf9* cell system. All vector lots were produced with AAV2 *Rep* and AAV2 ITRs with single-stranded genome configurations. Abbreviations: I = iodixanol gradient; MQ = MustangQ column; TFF = tangential flow filtration; S = 100-kDa MWCO filter.

Source	rAAV	Produced in	Purification	Lot #
UNC Chapel Hill	AAV1-CBA-GFP	HEK293	Column	AV6034
	AAV2-CBA-GFP			AV6035
	AAV5-CBA-GFP			AV6036
	AAV6-CBA-GFP			AV6037d
	AAV8-CBA-GFP			AV6038
	AAV9-CBA-GFP			AV6039
Virovek	AAV1-CMV-GFP	Baculo-*Sf9*	CsCl	15-621
	AAV2-CMV-GFP			16-017
	AAV6-CMV-GFP			13-195
	AAV8-CMV-GFP			14-365
	AAV9-CMV-GFP			15-409
UIowa	AAV1-CMV-eGFP	Baculo-*Sf9*	I-MQ	AAV2820
	AAV2-CMV-eGFP			AAV2601
	AAV5-CMV-eGFP			AAV2844
	AAV6-CMV-eGFP			AAV2588
	AAV8-CMV-eGFP			AAV2846
	AAV9-CMV-eGFP			AAV2646

Supplemental Table 5. Biomanufacturing facilities used to determine the universality of rAAV capsid thermal stability in different capsid serotypes in Figure S8b-d. Human rAAV vector lots manufactured at UNC were produced via transient plasmid transfection into suspension HEK293 cells in serum and antibiotic-free media. Insect rAAV vector lots manufactured at University of Iowa and Virovek were produced via live baculoviral infection of *Sf9* insect cells. All vector lots were produced with AAV2 *Rep* and AAV2 ITRs. Abbreviations: I = iodixanol gradient; MQ = MustangQ column; CsCl = cesium chloride density gradient; CBA = chicken b-actin promoter; CMV = cytomegalovirus promoter; GFP = green fluorescent protein.

Supplemental Table 6. All HCP impurities present in human and baculovirus-*Sf9* preparations of rAAV1. All HCP impurities identified by LC-MS/MS for rAAV1 from both cell lysate and media-purified vector preparations. Excluded from the list are common process contaminants that occur in routine sample preparation (human keratin, trypsin, etc.), and impurities with mutations/aberrations such that they didn't appear in the main search library. Searches were conducted against the complete proteomes of *Homo sapiens*, *Spodoptera frugiperda*, *Autographa californica multiple nuclepolyhedrovirus* (baculovirus), *Adeno-associated virus* serotype 1, and common process contaminants (BSA from the media, etc.). PSM = peptide spectral match.

[Table is an attached excel file].

Production	Source	HCP impurity peptide	Unmodified peptide mass (Da)	Modified peptide mass (Da)	Hex NAc	Hex	Me-HexA	Fuc
Transient transfection in human HEK293	Cell lysate	None	n/a					
	Media	None	n/a					
Live baculovirus infection of *Spodoptera frugiperda Sf9* insect cells	Cell lysate	KNYTVELHELEALAK (*Sf9* ferritin)	1757.9432	3136.4374	2	6		
				3298.4838	2	7		
				2796.3262	2	3		1
				2634.2782	2	2		1
				1961.0278	1			
		AKNYTVELHELEALAK (*Sf9* ferritin)	1828.9803	2867.3706	2	3		1
				2032.0702	1			
		NYTVELHELEALAK (*Sf9* ferritin)	1629.8483	3332.43926	2	8		
				3170.388	2	7		
				3008.3616	2	6		
				1832.934	1			

Supplemental Table 7. HCP impurities with N-linked glycans from human and baculo-*Sf9* produced preparations of rAAV1. N-linked glycans (modified residue is underlined) present on HCP impurities identified by LC-MS/MS for rAAV1 from both cell lysate and media-purified vector preparations. Excluded from the list are common process contaminants that occur in routine sample preparation (human keratin, trypsin, etc.), impurities with mutations/aberrations such that they didn't map to known proteins by BLASTp search, and any modification which could not be site-localized. HexNAc = N-acetylhexoseamine; Hex = hexose; Me-HexA = methylated hexuronic acid; Fuc = fucose.

rAAV	Source	Produced in	Cell or media	Purification	Titer (vg/mL)	Lot #
AAV1-EF1α-FLuc	UIowa	HEK293	Cell	I-MQ	1.50E+12	AAV3170
			Media	S-TFF-I-MQ	2.80E+12	AAV3174
		Baculo-*Sf9*	Cell	I-MQ	1.20E+13	AAV3168
			Media	S-TFF-I-MQ	2.40E+12	AAV3169

Supplemental Table 8. Viral specifications for the rAAV1 vector lots used in Figure S9. A single transfer vector plasmid lot (Fig S1) was used to produce vector in each system. Human rAAV vector lots were produced via the standard 3-plasmid transient transfection system in HEK293(FT) cells. Baculo-*Sf9* rAAV vector lots were produced via the baculovirus-infected *Sf9* cell system. All vector lots were produced with AAV2 *Rep* and AAV2 ITRs with single-stranded genome configurations. Abbreviations: I = iodixanol gradient; MQ = MustangQ column; TFF = tangential flow filtration; S = 100-kDa MWCO filter.

rAAV8 sample type	# of micrographs	# of particles	Resolution (Å)
HEK293 Full	1,645	63,471	3.3
HEK293 Empty	1,645	15,107	3.3
Baculo-*Sf9* Full	395	404	3.6
Baculo-*Sf9* Empty	395	2,359	3.3

Supplemental Table 9. Summary of cryo-EM processing parameters for the four new rAAV8 structures. Processing parameters for the four rAAV8 structures purified from cell lysates from each manufacturing platform, including both full (had a genome) and empty capsids (lacked an AAV genome). More detailed viral manufacturing specifications for the rAAV8 vector lots used are listed in Table S4. Å = angstrom.

Source	rAAV	Produced in	Purification	Lot #
UIowa	AAV1-CMV-eGFP	HEK293	I-MQ	AAV2762
	AAV5-CMV-eGFP		I-MQ	AAV2042
	AAV6-CMV-eGFP		CsCl	AAV2885
	AAV8-CMV-eGFP		I-MQ	AAV2337
	AAV1-CMV-eGFP	Baculo-*Sf9*	I-MQ	AAV2820
	AAV2-CMV-eGFP		I-MQ	AAV2601
	AAV4-CMV-eGFP		I-MQ	AAV2771
	AAV5-CMV-eGFP		I-MQ	AAV2844
	AAV6-CMV-eGFP		I-MQ	AAV2588
	AAV8-CMV-eGFP		I-MQ	AAV2846

Supplemental Table 10. Different rAAV capsid serotypes used to determine universality of capsid PTM deposition. Human rAAV vector lots were produced with the classic 3-plasmid transient transfection system in HEK293(FT) cells. Insect rAAV vector lots were produced via the baculovirus-infected *Sf9* cell system. All vector lots were produced with AAV2 *Rep* and AAV2 ITRs, had single-stranded genome configurations, were purified only from cell lysate from a single facility at the University of Iowa Viral Vector Core. Abbreviations: I = iodixanol gradient; MQ = MustangQ column; CsCl = cesium chloride density gradient.

Supplemental Table 11: PTMs present in human and baculovirus-*Sf9* preparations from various serotype vectors produced at a single facility in Table S10. Manually validated PTMs identified by LC-MS/MS for serotypes listed in Table S10. Position numbering is for each serotype, unaligned to the other serotypes. Modification types: [+0.98492] = deamidation of Asn and Gln; [+14.01565] = methylation; [+15.99492] = oxidation of Met (often the result of processing, not a real PTM); [+42.01057] = acetylation; [+71.03711] = propionamido-Cys; [+79.96633] = phosphorylation.

[Table is an attached Excel file].

Supplemental Table 12: HCP impurities present in human and baculo-*Sf9* preparations from various serotype vectors produced at a single facility in Table S10. HCP impurities identified by LC-MS/MS for all serotypes listed in Table S10 from cell lysate purified vector preparations. Excluded from the list are common process contaminants that occur in routine sample preparation (human keratin, trypsin, etc.). Searches were conducted against the complete proteomes of *Homo sapiens*, *Spodoptera frugiperda*, *Autographa californica multiple nuclepolyhedrovirus* (baculovirus), adeno-associated virus serotypes 1/2/4/5/6/8, and common process contaminants (BSA from the media, etc.). PSM = peptide spectral match.

[Table is an attached excel file].

Platform	AAV	Glycosylated HCP impurity peptide	Unmodified peptide mass (Da)	Modified peptide mass (Da)	Hex NAc	Hex	HexA	Fuc
Baculo-*Sf9*	AAV1	KNYTVELHELEALAK (*Sf9* ferritin)	1757.9436	1961.0236	1			
		NYTVELHELEALAK (*Sf9* ferritin)	1629.8483	2668.2303	2	3		1
				1832.9298	1			
	AAV5	NYTVELHELEALAK (*Sf9* ferritin)	1629.8483	2668.2303	2	3		1
				1978.9856	1			1
				1832.9298	1			
		KNYTVELHELEALAK (*Sf9* ferritin)	1757.9436	1961.0236	1			
		KNYTVELHELEALAK (*Sf9* ferritin)	1757.9436	1961.0236	1			
	AAV8	KNYTVELHELEALAK (*Sf9* ferritin)	1757.9436	1961.0236	1			
Human HEK293	AAV6	VQPFNVTQGK (human lysosomal membrane glycoprotein-2)	1117.6000	1320.6793	1			
		GHTLTLNFTR (human lysosomal membrane glycoprotein-1)	1159.6218	1362.7011	1			
		AGHTLTLNFTR (human lysosomal membrane glycoprotein-1)	1230.6589	1433.7382	1			
		AAIPSALDTNSSK (human galectin-3-binding protein precursor)	1274.6587	1477.738	1			
				1623.679	1			1
		TNSTFVQALVEHVK (human prosaposin)	1572.838	3314.4302	3	5	1	1
				2611.2132	2	3		1
				2449.1604	2	2		1
				1921.9764	1			1

Supplemental Table 13. Glycosylated HCP impurities from human and baculovirus-*Sf9* produced preparations of multiple AAV serotypes produced at one facility. N-linked glycans (modified residue is underlined) present on HCP impurities identified by LC-MS/MS for numerous common serotypes. Excluded from the list are common process contaminants that occur in routine sample preparation (human keratin, trypsin, etc.), impurities with mutations/aberrations such that they didn't map to known proteins by BLASTp search, and any modification that could not be site-localized. HexNAc = N-acetylhexoseamine; Hex = hexose; HexA = hexuronic acid; Fuc = fucose.

rAAV	Source	Produced in	Purification	Lot #
AAV1-CMV-FLuc	UPenn	HEK293	TFF-I-MQ	V2682TI
AAV1-CMV-rhCGB	SignaGen Labs	HEK293	CsCl	AAV61882
AAV2-CBA-GFP	UNC Chapel Hill	HEK293	CsCl	AV6108
AAV8-CBA-GFP	UNC Chapel Hill	HEK293	CsCl	AV4909
AAV8-CAG-TdTom	Stanford	HEK293T	CsCl	NPL1
AAV8-CAG-TdTom	Stanford	HEK293T	CsCl	NPL2
AAV8-CBA-GFP	ATCC reference strain	HEK293	CsCl	03112010SP2pcg
AAV8-CMV-FLuc	UPenn	HEK293	TFF-I-MQ	V5489L
AAV2-CMV-GFP	UIowa	Baculo-*Sf9*	TFF-I-MQ	AAV2601
AAV2-CMV-hAADC	UMass	Baculo-*Sf9*	AVB Sepharose	n/a
AAV8-CMV-GFP	UIowa	Baculo-*Sf9*	TFF-I-MQ	AAV2846
AAV8-CMV-GFP	Virovek	Baculo-*Sf9*	CsCl	15-129
AAV8-CMV-FLuc	Virovek	Baculo-*Sf9*	CsCl	16-255

Supplemental Table 14. List of biomanufacturing facilities used to determine the universality of rAAV capsid PTM deposition regardless of manufacturer or method. Human rAAV vector lots were produced via standard transient plasmid transfection into HEK293 cells. Insect rAAV vector lots were produced via live baculoviral infection of *Sf9* insect cells. All vector lots were produced with AAV2 *Rep* and AAV2 ITRs with single-stranded genome configurations. Note: ATCC lot was originally sourced from the University of Florida Powell Gene Therapy Center. Abbreviations: I = iodixanol gradient; MQ = MustangQ column; CsCl = cesium chloride density gradient; TFF = tangential flow filtration; rhCGB = rhesus chorionic gonadotropin; CBA = chicken b-actin promoter; TdTom = Td-Tomato; FLuc = firefly luciferase; CMV = cytomegalovirus promoter; hAADC = human aromatic L-amino acid decarboxylase.

Made In	rAAV	Source	Peptide	Position
Human HEK293	AAV8-GFP	ATCC	K.KRPVEP**S**[+79.96633]PQRSPDSSTGIGK.K	S149
			K.KRPVEPSPQR**S**[+79.96633]PDSSTGIGK.K	S153
	AAV1-rhCGB	SignaGen	K.**K**[+42.01057]RPVEQSPQEPDSSSGIGK.T	K143
			K.KRPVEQ**S**[+79.96633]PQEPDSSSGIGK.T	S149
			R.TQNQSGSAQN**K**[+14.01565]DLLFSRG.S	K459
			R.TQNQSGSAQNKDLLFS**R**[+14.01565]G.S	K465
	AAV2-GFP	UNC	K.KRPVEH**S**[+79.96633]PVEPDSSSGTGK.A	S149
	AAV8-TdTom	Stanford	R.TQTTGGTAN**T**[+79.96633]QTLGFSQGGPNTMANQAK.N	T460
			R.FFPSNGILIFG**K**[+14.01565]Q.N	K547
			K.NTPVPADPP**T**[+79.96633]TFNQSK.L	T662
	AAV8-TdTom	Stanford	**M**.[+42.01057]AADGYLPDWLEDNLSEGIR.E	M1
			M.[+42.01057]AADGYLPDWLEDNLSEGIREW.W	M1
			K.KRPVEP**S**[+79.96633]PQR.S	S149
			K.RPVEPSPQRSPDS**S**[+79.96633]TGIGK.K	S157
	AAV1-FLuc	U-Penn	**M**.[+42.01057]AADGYLPDWLEDNLSEGIREWWDLKPGAPKPKA.N	M1
			K.GEPVNAADAAALEHD**K**[+14.01565]AYDQQLKAG.D	K77
			K.**K**[+42.01057]RPVEQSPQEPDSSSGIGK.T	K143
			K.RPVEQ**S**[+79.96633]PQEPDSSSGIGK.T	S149
			M.ASH**K**[+42.01057]DDEDKFFPMSGVMIFGK.E	K528
	AAV8-FLuc	U-Penn	**M**.[+42.01057]AADGYLPDWLEDNLSEGIREWWALKPGAPKPK.A	M1
			K.KRPVEP**S**[+79.96633]PQR.S	S149
			R.NSLANPGIA**M**[+15.99492]ATH**K**[+42.01057]DDEERFFPSNGILIFGK.Q	K530
			M.ATH**K**[+42.01057]DDEERFFPS**N**[+0.98402]GILIFGK.Q	K530/N540
			K.TTNPVATEEYGIVADNLQQQNTAPQIGTVN**S**[+79.96633]QGALPGMVWQNR.D	S600
			Q.NRDV**Y**[+79.96633]LQGPIWAKIPHTDGNFHPSPLMGGFGLK.H	Y615
Baculo-*Sf9*	AAV8-GFP	Virovek	R.FFPS**N**[+0.98402]GILIFG**K**[+14.01565]Q.N	N540/K547
			R.DVYLQGPIWA**K**[+14.01565].I	K623
	AAV8-FLuc	Virovek	K.KRPVEP**S**[+79.96633]PQRSPDSS**T**[+79.96633]GIGK.K	S149/T158
			K.RPVEPSPQR**S**[+79.96633]PDSSTGIGK.K	S153
			K.YHLNGR**N**[+0.98402]**S**[+79.96633]LANPGIAMATHKDDEER.F	N517/S518
			R.FFPSNGILIFG**K**[+14.01565]Q.N	K547
			L.KHPPPQILI**K**[+14.01565]NTPVPADPPTTFNQSK.L	K652
	AAV2-hAADC	U-Mass	LQF**S**[+661.6639]QAGASDIRDQSR	S463
			VSK**T**[+788.7003]SADNNNSEYSWTGATK	T491
			LV(dN)PGPAMA**S**[+673.14]HKDDEEKFFPQSGVLIFGK	S525
	AAV2-GFP	U-Iowa	K.KRPVEH**S**[+79.96633]PVEPDSSSGTGK.A	S149
	AAV8-GFP	U-Iowa	R.NSLANPGIA**M**[+15.99492]ATH**K**[+42.01057].D	K530
			R.FFPSNGILIFG**K**[+42.01057]QNAAR.D	K547
			R.DNADYSDVMLT**S**[+79.96633]EEEIK.T	S564

Supplemental Table 15: PTMs present in human and baculovirus-*Sf9* preparations from vectors listed in Table S14. Manually validated PTMs identified by LC-MS/MS for vectors listed in Table S14 from both cell lysate and media-purified vector preparations. Position numbering is for each serotype, unaligned to the other serotypes. The bold amino acid preceding the bracket were modified with: [+0.98492] = deamidation of Asn and Gln; [+14.01565] = methylation; [+15.99492] = oxidation of Met (often the result of processing, not a real PTM); [+42.01057] = acetylation; [+79.96633] = phosphorylation; [+661.6639/673.14/788.7003] = O-linked (Ser/Thr) N-acetylhexoseamine.

Supplemental Table 16: HCP impurities present in human and baculovirus-*Sf9* preparations from vectors listed in Table S14. HCP impurities identified by LC-MS/MS for all serotypes and vectors listed in Table S14 from both cell lysate and media-purified vector preparations. Excluded from the list are common process contaminants that occur in routine sample preparation (human keratin, trypsin, etc.). Searches were conducted against the complete proteomes of *Homo sapiens*, *Spodoptera frugiperda*, *Autographa californica multiple nuclepolyhedrovirus* (baculovirus), *Adeno-associated virus* serotypes 1/2/8, and common process contaminants (BSA from the media, etc.). PSM = peptide spectral match.

[Table is an attached excel file].

Supplemental Table 17: Cumulative human HCP impurities present in all human-produced rAAV vector preparations tested to date. Cumulative combined list of all human HCP impurities identified by LC-MS/MS for all human-produced vectors from both cell lysate and media-purified vector preparations. Excluded from the list are common process contaminants that occur in routine sample preparation (human keratin, trypsin, etc.). PSM = peptide spectral match.

[Table is an attached excel file].

Supplemental Table 18: Cumulative *Sf9* HCP impurities present in all baculo-*Sf9* produced rAAV vector preparations tested to date. Cumulative combined list of all *Sf9* HCP impurities identified by LC-MS/MS for all baculo-*Sf9* produced vectors from both cell lysate and media-purified vector preparations. Excluded from the list are common process contaminants that occur in routine sample preparation (human keratin, trypsin, etc.). PSM = peptide spectral match.

[Table is an attached excel file].

Supplemental Table 19: Cumulative baculoviral HCP impurities present in all baculo-*Sf9* produced rAAV vector preparations tested to date. Cumulative combined list of all baculoviral HCP impurities identified by LC-MS/MS for all baculo-*Sf9* produced vectors from both cell lysate and media-purified vector preparations. Excluded from the list are common process contaminants that occur in routine sample preparation (human keratin, trypsin, etc.). PSM = peptide spectral match.

[Table is an attached excel file].

Serotype	ER signal peptide	Position
AAV1	Dx(1)E [HK]x(1)K	96-99 30-33, 74-77
AAV2		96-99 23-26, 74-77
AAV3b		96-99 74-77
AAV4		95-98 29-32, 73-76
AAV5		95-98 29-32
AAV6		96-99 30-33, 74-77
AAV8		96-99 30-33, 74-77
AAV9		96-99 74-77
AAV12		96-99 74-77

Supplemental Table 20. Putative ER signal peptides are conserved in all natural rAAV VP1 polypeptides. Putative ER signaling peptides were assessed for their presence on the N-terminal VP1 sequence of known natural AAV serotypes. Dx(1)E refers to Asp-x-Glu where 'x' represents any amino acid, and (1) refers to the number of times the preceding sequence can occur. HK]x(1)K refers to His-Lys-x-Lys where 'x' represents any amino acid, and (1) refers to the number of times the preceding sequence can occur.

Index 1	Index 2
TCAGTGGCGAGT	AAAGTATGCTAC
CCGCCGCAAGAA	AAAGGGAGCGTG
CTCGGGACTGTT	TAAGCAAAGCAA
TAGGGATGTAAT	ATAGATAGTTCC
GAAATCAAGCGG	TCTATGACCATC
TTTGGGTTGAAT	CAAATACACTGA
CGGGTCCTAAAC	ATTCGGATTACA
TTTCAGGCACTC	CTAAAGGTCAAA

Supplemental Table 21: Indices used for NGS sequencing of packaged rAAV genomes. Sequencing indices placed within the i5 and i7 adapters to enable dual-indexed pooled Illumina sequencing via Fast-Seq.

Metric	BM1	HM1	HC8	BM8	BC1	HC1	BC8	HM8
Genome size (bp)	4,364	4,364	4,364	4,364	4,364	4,364	4,364	4,364
Mean coverage	2,851	3,080	1,395	1,145	1,936	2,545	1,734	1,659
Median coverage	2,587	2,524	1,238	930	1,661	1,973	1,408	1,380
Genome coverage range, not including ITRs	849 - 11,052	850 - 10,194	164 - 6,410	160 - 4,935	578 - 6,701	540 - 10,869	324 - 7,321	230 - 11,479
Genome coverage range of ITRs	190 - 2,110	135 - 1,778	38 - 1,193	28 - 1,112	96 - 1,451	74 - 1,411	81 - 1,641	51 - 989
Number of SNPs	0	0	0	0	0	0	0	0
Number of MNPs	0	0	0	0	0	0	0	0
Number of indels	0	0	0	0	0	0	0	0
Number of others (SVs)	0	0	0	0	0	0	0	0
Number of multiallelic sites	0	0	0	0	0	0	0	0
Number of multiallelic SNP sites	0	0	0	0	0	0	0	0

Supplemental Table 22: Comparative metrics for NGS sequencing of packaged rAAV genomes including ITRs. Metrics reported from Fast-Seq demonstrating no difference in the packaged genomes between vectors or serotypes packaged in either manufacturing platform. BM = baculo-*Sf9* media purified; HM = human media purified; HC = human cell purified; BC = baculo-*Sf9* cell purified; SV = structural variant; SNP = single nucleotide polymorphism; MNP = multi nucleotide polymorphism.

rAAV	Source	Produced in	Cell or media	Purification	Titer (vg/mL)	Lot #
AAV1-CMV-FLuc-SV40pA	UPenn	HEK293	Media	TFF-I-MQ	7.06E+12	V2682TI
	Virovek	Baculo-*Sf9*	Cell	CsCl	2.28+13	15-093
AAV8-CMV-FLuc-SV40pA	UPenn	HEK293	Media	TFF-I-MQ	7.89E+13	V5489L
	Virovek	Baculo-*Sf9*	Cell	CsCl	2.37E+13	16-255

Supplemental Table 23. Viral specifications for the rAAV1 and rAAV8 vector lots used in Figure 3e,f. A ssCMV-FLuc-SV40pA transfer vector was used at each facility. Human rAAV vector lots were produced via the standard 3-plasmid transient transfection system in HEK293 cells. Baculo rAAV vector lots were produced via the baculovirus-infected *Sf9* cell system. All vector lots were produced with AAV2 *Rep* and AAV2 ITRs with single-stranded genome configurations. Abbreviations: I = iodixanol gradient; MQ = MustangQ column; TFF = tangential flow filtration; CsCl = cesium chloride density gradient.

Supplemental Table 24: Database of all approved advanced biologic therapies that contain proteins in their formulation. Detailed list of the 373 approved protein-containing advanced therapy medicinal products for use in humans (number is as of date of publication). Includes vaccines, antibodies, antibody-drug conjugates, immune globulins, anti-venoms and anti-toxins, gene and cell therapies, hormones, blood products and enzymes separated into different tabs based on therapy type. Listed for each therapeutic are the name (including trade names and proper names), cell line and species of production, manufacturer, approval year, target/indication, and in some cases the route of administration.

[Table is an attached excel file].